Title:

Netrin signaling mediates survival of dormant epithelial ovarian cancer cells

Authors:

Pirunthan Perampalam[1,2], James I. MacDonald[1,3], Komila Zakirova[1,3], Daniel T. Passos[1,3], Sumaiyah Wasif[1,3], Yudith Ramos-Valdes[1,4], Maëva Hervieu[5], Patrick Mehlen[5,6], Rob Rottapel[7,8], Benjamin Gibert[5], Rohann Correa[1,9], Trevor G. Shepherd[1,4,9,10,11], Frederick A. Dick[1,3,9,12,13]

Affiliations:

1. London Regional Cancer Program, London Health Sciences Centre Research Institute, London, Ontario, Canada, N6A 4L6.
2. Department of Biochemistry, University of Western Ontario, London, ON, Canada, N6A 5C1.
3. Department of Pathology and Laboratory Medicine, University of Western Ontario, London, ON, Canada, N6A 5C1.
4. The Mary and John Knight Translational Ovarian Cancer Research Unit, London Regional Cancer Program, London, Ontario, Canada, N6A 4L6.
5. Apoptosis, Cancer and Development Laboratory - Equipe labellisée 'La Ligue', LabEx DEVweCAN, Institut Convergence PLAsCAN, Centre de Recherche en Cancérologie de Lyon (CRCL), INSERM U1052-CNRS UMR5286, Université de Lyon, Université Claude Bernard Lyon1, Centre Léon Bérard, 69008 Lyon, France.
6. Netris Pharma, 69008 Lyon, France
7. Princess Margaret Cancer Centre, University Health Network, 101 College Street, Toronto, Ontario, Canada, M5G 1L7
8. Department of Medical Biophysics, University of Toronto, 1 King's College Circle, Toronto, Ontario, Canada, M5S 1A8
9. Department of Oncology, Western University, London, Ontario, Canada, N6A 4L6.
10. Department of Obstetrics and Gynecology, Western University, London, Ontario, Canada, N6A 5W9.
11. Department of Anatomy and Cell Biology, Western University, London, Ontario, Canada, N6A 5C1.
12. Children's Health Research Institute, London, Ontario, Canada, N6A 4V2.
13. Correspondence: fdick@uwo.ca

Keywords:
Netrin, high grade serous ovarian cancer, DYRK1A, dormancy, quiescence, spheroids

Conflict of interest statement:
P. Mehlen is the founder and CEO of Netris Pharma and has an ownership interest including stocks and patents. The other authors have declared that no conflict of interest exists.

Abstract

Dormancy in cancer is a clinical state in which residual disease remains undetectable for a prolonged duration. At a cellular level, rare cancer cells cease proliferation and survive chemotherapy and disseminate disease. We created a suspension culture model of high grade serous ovarian cancer (HGSOC) dormancy and devised a novel CRISPR screening approach to identify survival genes in this context. In combination with RNA-seq, we discovered the Netrin signaling pathway as critical to dormant HGSOC cell survival. We demonstrate that Netrin-1, -3, and its receptors are essential for low level ERK activation to promote survival, and that Netrin activation of ERK is unable to induce proliferation. Deletion of all UNC5 family receptors blocks Netrin signaling in HGSOC cells and compromises viability during the dormancy step of dissemination in xenograft assays. Furthermore, we demonstrate that Netrin-1 and -3 overexpression in HGSOC correlates with poor outcome. Specifically, our experiments reveal that Netrin overexpression elevates cell survival in dormant culture conditions and contributes to greater spread of disease in a xenograft model of abdominal dissemination. This study highlights Netrin signaling as a key mediator HGSOC cancer cell dormancy and metastasis.

56 **Introduction**

57 Relapse from initially effective cancer treatment represents one of the greatest barriers to
58 improving outcomes (1). Dormant or minimal residual disease that is not clinically detectable is
59 a common source of relapse, particularly in a metastatic setting (2). This has motivated the
60 search for, and study of, disseminated cancer cells. Cellular dormancy has been characterized in
61 cancer cells derived from a variety of primary disease sites including breast, prostate, melanoma,
62 and others (3, 4). Disseminated cells often occupy specific cellular niches in perivascular space
63 or in bone marrow (5). They adopt catabolic metabolism (2), and withdraw from the cell cycle
64 (4). Stem like phenotypes and epithelial to mesenchymal transition also characterize the biology
65 of these cells as they survive dissemination and lay quiescent in distant tissues (1, 3, 5). Across a
66 variety of disease sites this dormant state is characterized by diminished Ras-MAPK signaling
67 and elevated p38 activity (3, 6). To develop treatments specifically tailored for dormant cells, a
68 systematic search for vulnerabilities unique to dormancy is needed. To this end, high grade
69 serous ovarian cancer (HGSOC) disseminates in ascites as growth arrested cellular aggregates
70 (7). This has been modeled in culture (8), and studies confirm active induction of cell cycle arrest
71 mechanisms (9, 10), induction of autophagy (11, 12), and other known characteristics of
72 dormancy (13). This suggests that HGSOC spheroids are ideal to search for survival
73 dependencies specific to dormant cells.

74 High grade serous ovarian cancer (HGSOC) is the deadliest gynecologic malignancy,
75 accounting for more than 70% of cases (14). Its poor prognosis is largely attributed to late-stage
76 diagnosis with metastases already present. Metastatic spread is facilitated by multicellular
77 clusters of tumor cells, called spheroids, that are shed into the peritoneal cavity and disseminate
78 to nearby organs (15). The non-proliferative state of spheroid cells renders them chemoresistant

79 and contributes to disease recurrence, emphasizing the need to understand the biology of these
80 cells (16). Dormant HGSOC cells are characterized by similar metabolic changes, EMT, and
81 cytokine signaling as dormant cancer cells from other disease sites (3, 13). Mechanisms that
82 mediate their dormant properties include AMPK-LKB1 signaling that induces autophagy (17,
83 18), STAT3 and FAK for survival and chemoresistance (19, 20), and DYRK1A signaling to
84 arrest proliferation (10). Unfortunately, therapeutic approaches to target these pathways in
85 ovarian cancer have yet to emerge, indicating that more candidates are needed.

86 Netrins are a family of secreted factors that reside in the extracellular matrix and were
87 first identified in axon guidance in the developing nervous system (21, 22). Together with their
88 receptors, Netrins have since been implicated in cancer progression (23). Netrin-1 is the most
89 studied and its misregulation in cancer leads to pro-survival signals (24). Netrin interactions
90 with DCC and UNC5 homologs (UNC5H, UNC5A-D) convert pro-death signals by these
91 dependence receptors to survival signals (25). Netrin signals through PI3K-AKT and ERK-
92 MAPK are known to participate in orientation decisions in development by providing guidance
93 cues (26-28), while loss of ligand binding leads DCC or UNC5H to stimulate dephosphorylation
94 of DAPK1 that sends pro-death signals (29, 30). The gene encoding DCC is frequently deleted
95 in cancer (24), and Netrin-1 blocking antibodies are in Phase II clinical trials for endometrial and
96 cervical carcinomas to inhibit metastatic growth (25). Alternative receptors for Netrins such as
97 NEO, DSCAM, and Integrins also mediate their signals (23), creating a myriad of possible
98 pathways for Netrins to regulate cancer cells. Lastly, functional roles for Netrin-3, -4, and -5 are
99 still relatively unexplored compared to Netrin-1 (31), although their expression patterns suggest
100 roles in advanced forms of some cancers (32). A functional role for Netrins and their receptors
101 in dormancy, or other aspects of HGSOC spheroid biology have yet to be reported.

102 In this study we utilized a suspension culture system to interrogate survival mechanisms
103 in dormancy using HGSOC spheroids. To maximize discovery of gene loss events that
104 compromise viability in dormancy, we devised a novel genome-wide CRISPR screen approach
105 that we term 'GO-CRISPR'. In addition to the standard CRISPR workflow, GO-CRISPR
106 utilizes a parallel screen in which 'guide-only' cells lacking Cas9 are used to control for
107 stochastic changes in gRNA abundance in non-proliferative cells. This screen identified multiple
108 Netrin ligands, DCC, UNC5Hs, and downstream MAPK signaling components as supporting
109 survival of HGSOC cells in dormant culture conditions. A transcriptomic analysis of HGSOC
110 spheroids also revealed Netrin signaling components were enriched in HGSOC spheroids
111 compared to adherent cells, and that in the absence of the DYRK1A survival kinase Netrin
112 transcriptional increases were lost. We show that multiple Netrins, UNC5 receptors, and the
113 downstream MEK-ERK axis is crucial for survival signaling in dormant cell culture.
114 Importantly, Netrin activation of ERK is restricted to spheroid cultures and is unable to stimulate
115 proliferation, consistent with its role in dormant survival. We blocked Netrin signaling by
116 deleting UNC5 receptors and using xenograft approaches demonstrated that loss of Netrin
117 signaling compromises survival of HGSOC cells, specifically in the dormant stage of
118 dissemination. Furthermore, we show that overexpression of Netrin-1 and -3 are associated with
119 poor prognosis in HGSOC and their overexpression in culture increases survival in suspension
120 culture. Netrin overexpression in xenografts contributes to increased disease dissemination in a
121 model of metastasis. Our study highlights Netrin-ERK signaling as a requirement for spheroid
122 survival and suggests it may be a potential therapeutic target for eradicating dormant HGSOC
123 cells.

124 **Results**

125 ***Axon guidance genes are essential factors for HGSOC spheroid viability***

126 To dissect genetic dependencies of dormant ovarian cancer cells, we utilized a suspension
127 culture system that encourages cellular aggregation, leading to non-proliferative spheroids that
128 resemble dormant aggregates found in ovarian cancer patient ascites (7, 10, 13, 33). **Fig. 1A**
129 illustrates withdrawal from cellular proliferation by HGSOC cells in suspension as evidenced by
130 reduced expression of Ki67 and increased expression of the quiescence marker p130 (34).
131 Furthermore, phospho-western blots for ERK demonstrate reduced but not absent
132 phosphorylation, and phospho-p38 either remains consistent or is increased. Reduced phospho-
133 ERK and elevated phospho-p38 are indicative of the characteristic signaling switch reported to
134 underlie most paradigms of cancer cell dormancy (5). These findings are relatively consistent
135 among the three HGSOC cell lines; iOvCa147, OVCAR8, TOV1946 selected for use in our
136 screen. To discover genes required for survival in spheroids, we utilized a new approach called
137 GO-CRISPR (Guide Only CRISPR) that we developed specifically for survival gene discovery
138 in three-dimensional spheroid cell culture conditions (**Fig. 1B**). GO-CRISPR incorporates
139 sgRNA abundances from non-Cas9-expressing cells to control for stochastic (non-Cas9
140 dependent) effects that are a challenge in three-dimensional culture conditions with slow or
141 arrested proliferation (35). We used sequencing to determine sgRNA identity and abundance in
142 the library, initially infected cells, and in cells following 48 hours of suspension culture (**Fig.
143 1B**). Read count data was analyzed using a software package that we developed to analyze GO-
144 CRISPR data (summarized in **Fig. 1 -Fig. Sup. 1A&B**). We selected genes that had a
145 Spheroid/Adherent Enrichment Ratio (ER) less than 1 ($P<0.05$) because some genes become
146 depleted in adherent growth before being transferred to suspension culture conditions and this

147 ratio selects for genes with a stronger effect in suspension when cells are not proliferating (**Fig.**
148 **1B**). To assess reliability of screen data, we investigated the classification of non-targeting
149 control sgRNAs. We computed a receiver operator characteristic curve (ROC) and determined
150 the area under the curve for each cell line (**Fig. 1 -Fig. Sup. 1C**). Greater than 95% of sgRNAs
151 in iOVCA147 and OVCAR8 screens were classified as non-essential, while 83% of sgRNAs in
152 TOV1946 cells were non-essential. In addition, we compared GO-CRISPR screen ER values
153 with viability data from siRNA knock down for 35 individual genes we have previously studied
154 in spheroid survival assays in OVCAR8 and iOVCA147 cells (**Fig. 1 -Fig. Sup. 1D**)(10). This
155 revealed a statistically significant correlation between the two sets of data, suggesting that genes
156 we previously knew supported spheroid viability (or were dispensable) were classified similarly
157 by our screen. These controls suggested our screen data was reliable for identifying new survival
158 dependencies.

159 We found 6,717 genes with an ER below 1 in iOvCa147 cells; and 7,637 genes in
160 TOV1946; and 7,640 genes in OVCAR8 cells. Among these genes; 1,382 were common to all
161 three cell lines (**Fig. 1D**). We performed pathway enrichment analysis on these common genes
162 and identified several significantly enriched pathways. These include primary and secondary
163 Reactome gene sets such as signal transduction, metabolism, and signaling by GPCR (**Fig. 1E**).
164 In addition, we identified a tertiary category called 'axon guidance,' that includes numerous
165 components of the Netrin signaling pathway that scored highly.

166

167 ***Expression of Netrin ligands and receptors are enriched in HGSOC spheroids***

168 DYRK1A was previously discovered to support survival of ovarian cancer cells in
169 suspension culture (10). Since DYRK1A phosphorylates RNA polymerase II in transcription
170 initiation (36), we sought to determine if it regulates gene expression in spheroid survival. We
171 created *DYRK1A*$^{-/-}$ iOvCa147 cells and confirmed their deficiency for survival in suspension
172 (**Fig. 2 -Fig. Sup. 1A-E**). Using iOvCa147 and *DYRK1A*$^{-/-}$ derivatives, we performed RNA-seq
173 on adherent and spheroid cells. We collected spheroids following a 6-hour incubation in
174 suspension because overexpression of known cell cycle transcriptional targets due to DYRK1A
175 loss were first evident at this time point, but loss of viability due to DYRK1A deficiency had not
176 yet occurred (10). We compared iOvCa147 adherent cells to 6-hour suspension culture to
177 identify transcriptional changes that occur as these cells transitioned from adherent conditions to
178 suspension conditions (**Fig. 2A**). We identified 1,834 genes that were upregulated, and pathway
179 enrichment analysis identified many of the same categories as our CRISPR screen including
180 axon guidance (**Fig. 2B**). We then compared iOvCa147 spheroid cells to *DYRK1A*$^{-/-}$ spheroid
181 cells to identify mRNA expression changes that were lost through DYRK1A deficiency (**Fig.
182 2C**). We identified 744 genes that were downregulated and these also belonged to many of the
183 same pathways, including axon guidance (**Fig. 2D**).

184 We compared enriched pathways from these two RNA-seq analyses with those that were
185 identified in our GO-CRISPR screens to identify gene expression programs in spheroids whose
186 products are essential for cell survival. 78 Reactome pathways were commonly enriched across
187 the GO-CRISPR screens and transcriptomic analyses, including 78 of the 83 pathways identified
188 in RNA-seq from *DYRK1A*$^{-/-}$ spheroid cells (**Fig. 2E**). The axon guidance pathway was one of
189 the most enriched among these common pathways (**Fig. 2F**). These data reveal that our GO-
190 CRISPR screen and transcriptomic analyses converge on this highly specific tertiary Reactome

191 category of axon guidance alongside much broader primary or secondary gene sets. This
192 category includes Netrin ligands, receptors, and downstream signaling components, suggesting a
193 previously unappreciated role in HGSOC spheroid viability.

194 We separately sought to confirm elevated expression of Netrins and some of their
195 signaling components in HGSOC spheroid cell culture. We examined expression levels of
196 ligands and receptors in the three cell lines used in our GO-CRISPR screen using RT- qPCR
197 (**Fig. 3A-C**). The precise identities of upregulated genes varies between cell lines, however each
198 cell line increases expression of some Netrins, at least one UNC5, and at least one of DCC,
199 DSCAM, and Neogenin. This suggests that the Netrin pathway components are expressed in
200 HGSOC cells may play a previously unappreciated role in dormancy and disease progression.

201 Since Netrin signaling has not been previously associated with dormancy we examined
202 expression of Netrin-1 and -3 ligands in spheroids isolated directly from patient ascites by
203 immunohistochemistry. First, we assessed proliferative markers in HGSOC tumor tissue and
204 spheroids by staining for Ki67 and p130. As expected, solid HGSOC tumors display uniform
205 Ki67 positivity and relative absence of p130 (**Fig. 4A-B**). Conversely, serial sections of
206 spheroids demonstrated rare Ki67 nuclear staining and abundant and uniform p130 staining.
207 This indicates that cells in these patient derived spheroids are quiescent (**Fig. 4C-E**). To
208 investigate the presence of Netrins, we initially tested Netrin-1 and -3 antibody specificity using
209 spheroids generated from OVCAR8 cells bearing knock out or over expression of Netrins (**Fig. 4**
210 **-Fig. Sup. 1A-F**). Dormant patient derived spheroids were stained for Netrins and epithelial
211 markers Cytokeratin and EpCAM. Since HGSOC is characterized by point mutations in p53 and
212 its accumulation in the nucleus, sections were also stained for p53 to confirm cancer cell identity
213 within these spheroids by high level nuclear staining (**Fig. 4F-H**). Overall, this confirms Netrin

214 expression occurs in dormant HGSOC patient spheroids, precisely the context our screen
215 indicates that they are critical for cell survival.

216

217 ***Netrin signaling stimulates ERK to support HGSOC spheroid survival.***

218 Netrin ligands and their dependence receptors are best known for their roles in axon
219 guidance (37), but are appreciated to regulate apoptosis in cancer (23). **Fig. 5A** illustrates
220 components of Netrin signaling and the frequency with which they were discovered to have an
221 ER of <1 in our screens. In addition, intracellular signaling molecules known to be downstream
222 of Netrin receptors that are shared with other enriched pathways identified in our screens, are
223 also illustrated. To confirm screen findings, we independently knocked out *NTN1*, *NTN3*, *NTN4*,
224 *NTN5*, the UNC5H receptor homologs (*UNC5A*, *UNC5B*, *UNC5C*, and *UNC5D*), as well as
225 *DCC*, *DSCAM*, and *NEO1* alone or in multigene combinations using lentiviral delivery of
226 sgRNAs and Cas9 (**Fig. 5 -Fig. Sup. 1A-C**). We assessed the effect of their loss on spheroid
227 survival in six HGSOC cell lines (iOvCa147, TOV1946, OVCAR3, OVCAR4, OVCAR8, and
228 COV318). Loss of at least one Netrin ligand resulted in reduced spheroid cell survival in five of
229 six cell lines (**Fig. 5B**). Notably, Netrin-3 loss showed the most pronounced effect on survival.
230 Cell lines such as OVCAR8 and COV318 were relatively resistant to the deletion of Netrin
231 pathway components as individual UNC5, *DCC*, and *DSCAM* genes rarely affected viability
232 (**Fig. 5B**). In these instances, combined deletions of UNC5 family members, or
233 *DCC;DSCAM;NEO1* (DDN for short) were either inviable or highly sensitive to suspension
234 culture induced cell death, suggesting redundancy in this pathway in some cell lines. Other cell
235 lines, such as OVCAR3, were highly sensitive to the loss of multiple individual ligands and any
236 individual UNC5H receptor was highly sensitizing to death induction in suspension (**Fig. 5B**).

237 Overall, these illustrate a robust role for Netrins in survival in this dormant cell culture assay.
238 Importantly, loss of receptor expression does not elevate viability as expected for a dependence
239 receptors, nor does it induce DAPK1 dephosphorylation (**Fig. 5 -Fig. Sup. 1D**), suggesting that
240 Netrin receptors in HGSOC spheroids transmit positive survival signals.

241 To determine if Netrin dependent signaling is active in HGSOC spheroids, we stimulated
242 cells in suspension with recombinant Netrin-1 (**Fig. 5C**). Western blotting for phospho-ERK, as
243 a measure of activation, revealed stimulation of MEK-ERK signaling in each of the cell lines
244 tested. Because MAPK signaling is best known for its role in proliferation, we also tested Netrin-
245 1 stimulation of quiescent, adherent cells and compared this with stimulation in spheroid culture.
246 Both conditions display similar, low levels of phospho-ERK, but Netrin-1 was only able to
247 stimulate ERK phosphorylation in suspension (**Fig. 5D**). Importantly, stimulation of adherent
248 cells with an equivalent concentration of EGF induced pERK levels commonly seen in
249 proliferating cells. Collectively, the context and magnitude of pERK stimulation by Netrin-1 is
250 inconsistent with proliferative signaling, suggesting it may contribute to survival. This suggested
251 that Netrin is a candidate pathway to provide low level, but essential survival signals through the
252 MAPK pathway in dormant spheroids. We investigated the dependence of ERK phosphorylation
253 on UNC5H and DDN receptors and discovered that it is lower when receptors are deleted (**Fig.
254 5E**). Furthermore, Netrin-1 stimulation of suspension cultures of OVCAR8 cells, or derivatives
255 deleted for UNC5 family members or DDN receptors, indicated that Netrin receptors are
256 essential to activate ERK in suspension culture (**Fig. 5F**). To confirm that Netrin-MEK-ERK
257 signaling contributes to survival in suspension culture, we used two different MEK inhibitors,
258 PD184352 and Trametinib, to treat OVCAR8 suspension cultures and observed that it causes
259 loss of cell viability in suspension culture (**Fig. 5G**). Since we routinely use reattachment of

260 spheroids to adherent plastic as a test of viability, also tested viability using trypan blue dye
261 exclusion to confirm that Trametinib is truly killing cells in suspension and it revealed the same
262 conclusion (**Fig. 5H**). As expected, treatment of cells in suspension with Trametinib lead to
263 lower phospho-ERK levels (**Fig. 5I**). The simplest explanation of this data is that Netrins signal
264 through a heterodimer or multi-receptor complex containing both an UNC5 and DDN component
265 that provides low level stimulation for MEK and ERK specifically in dormant culture conditions.

266 ***Netrin signaling is essential for dormant spheroid survival during metastatic dissemination***

267 To investigate the role of Netrin signaling in the context of residual disease and relapse, we
268 xenografted mice with control OVCAR8L cells, or UNC5 4KO cells, by intraperitoneal injection
269 (**Fig. 6A**). Two weeks following injection, mice were euthanized, and spheroids were obtained
270 by washing the abdominal cavity with PBS. Importantly, at this early stage of engraftment, solid
271 tumor lesions were not yet observable, indicating that we are modeling minimal residual disease
272 where dormancy is most relevant. Extraction of RNA from control OVCAR8 cell spheroids
273 recovered at this time point indicates a reduction in expression of pro-proliferative genes
274 compared to the same cells prior to engraftment (**Fig. 6B**). Furthermore, comparison with RT-
275 qPCR measurements of these same markers in suspension culture induced OVCAR8 spheroids
276 indicates that spheroids from abdominal washes are equivalently withdrawn from the cell cycle
277 (**Fig. 6, -Fig. Sup. 1**). This suggests spheroids at this stage are dormant. Furthermore, recovery
278 of spheroids by replating on adherent plastic indicates that deletion of UNC5 receptors to block
279 Netrin signaling extensively reduces survival under these circumstances (**Fig. 6C**). We also
280 quantitated cancer cells in these abdominal washes by qPCR using human Alu repeat detection to
281 count cells and this also demonstrates that cancer cell abundance is reduced in this dormant state
282 by loss of UNC5 receptors. Further xenografts were performed to investigate the long term

283 consequences of reduced survival of UNC5 4KO cells in mice. This demonstrated that mice
284 engrafted with UNC5 4KO cells had a considerably longer survival than control OVCAR8
285 recipient mice that received the same number of cells (**Fig. 6E,F**). Collectively, this
286 demonstrates that inhibition of Netrin signaling compromises viability and eventual disease
287 progression in a model of dormancy and dissemination.

288 ***Netrin overexpression is correlated with poor outcomes in HGSOC.***

289 Genomic studies indicate that HGSOC is one of the most aneuploid cancers (38). In
290 addition to the frequency of copy number variants per tumor, the locations of gains and losses
291 are dissimilar between cases, making this a highly heterogenous disease. Evaluation of TCGA
292 genomic data for HGSOC indicates rare amplifications or deletions of Netrin or Netrin-receptor
293 genes (**Fig. 7 -Fig. Sup. 1A**). Because of redundancy of Netrins and their receptor families this
294 data suggests HGSOC cases with deficiency for Netrin signaling are rare. This is consistent with
295 our data that all six cell lines tested reveal evidence of Netrin component dependence for
296 survival (**Fig. 5B**). Some TCGA HGSOC cases display elevated gene expression for Netrins or
297 their receptors, but only rare cases display low expression (**Fig. 7 -Fig. Sup. 1B**). This suggests
298 that Netrin signaling in HGSOC is retained despite high copy number variation in this cancer
299 type and there is occasional overexpression.

300 In agreement with our experimental data that multiple Netrin ligands can contribute to
301 spheroid survival in HGSOC (**Fig. 5A&B**), sorting cases by high level expression of Netrin-1
302 and -3 ligands reveals a significantly shorter overall survival compared to cases with low level
303 expression and this trend is also evident in the cases that only overexpress Netrin-3 (**Fig. 7A**).
304 This genomic data supports the interpretation that Netrin signaling is retained in HGSOC and its
305 elevation is deleterious to patient outcome.

306 We investigated overexpression of Netrin-1 and -3 in spheroid survival by generating
307 OVCAR8 derivatives that stably overexpress these proteins (**Fig. 7B**). We then utilized these
308 cells in suspension culture assays for spheroid survival as before (**Fig. 7C**). This data indicates
309 that overexpression of either Netrin-1 or -3 increases OVCAR8 cell survival in dormant spheroid
310 culture conditions. Examination of fixed spheroids isolated from this experiment further
311 indicates that elevated survival in this experiment is explained by an increase in abundance of
312 individual spheroids that overexpress either Netrin-1 or -3 (**Fig. 7D**). These experiments reveal
313 the significance of a previously undiscovered role for Netrins in HGSOC. High level expression
314 correlates with poor outcome and in suspension culture, overexpression confers oncogenic
315 properties on HGSOC cells.

316 ***Netrin overexpression induces abdominal spread of HGSOC.***

317 Our findings from CRISPR screens and cell culture experiments indicate that Netrin
318 signaling supports dormant HGSOC cell survival. Our analysis of TCGA is also predictive of a
319 worse outcome for patients. We sought to solidify these findings by searching for how Netrin
320 signaling affects HGSOC disease pathogenesis.

321 We utilized a xenograft assay in which OVCAR8 cells overexpressing Netrin-1 or -3
322 were injected into the peritoneal cavity and compared with OVCAR8 cells bearing an empty
323 vector as control. Mice were harvested following 35 days to analyze disease dissemination and
324 characterize the effect of Netrins in this model of HGSOC metastatic spread (**Fig. 8A**). Necropsy
325 of all animals at endpoint allowed for the identification and quantitation of tumor nodules within
326 the abdomen (**Fig. 8B**). Petal plots illustrate the frequency of specific organ and tissue sites
327 displaying tumor nodules (**Fig. 8B**). This revealed that spread to the omentum was similar across
328 all genotypes of xenografted cells and it occurred in all mice (**Fig. 8B**). In contrast, tumor

329 nodules were detected with increased abundance on the diaphragm, the liver, and mesenteries
330 that support the uterus (mesometrium) (**Fig. 8B**). In addition to more frequent disease spread to
331 these locations caused by Netrin overexpressing cells, we note that the quantity of nodules was
332 also increase in comparison with OVCAR8 control cells (**Fig. 8C-F**). We confirmed the source
333 of these lesions to be the xenografted cells using immunohistochemical staining for human
334 cytokeratin (**Fig. 8G,H**). Lastly, Netrin-1 and -3 histochemical staining confirms its presence in
335 the local tumor microenvironment (**Fig. 8G,H**). The similarity of increased tumor nodules seen
336 in xenografts and elevated spheroid formation and viability seen in culture suggests that Netrin
337 signaling improves cell viability in spheroid aggregates in vivo leading to increased disease
338 spread.

339

340 **Discussion**

341 In this report we investigated survival mechanisms in a model of HGSOC dormancy. We
342 utilized a modified CRISPR screening approach that was adapted to discover gene loss events in
343 largely non-proliferative conditions. We compared essential genes discovered in the screen with
344 gene expression increases identified by RNA-seq in dormant HGSOC cultures. This implicated
345 the Netrin signaling pathway in HGSOC spheroid survival. We independently validated the role
346 of Netrins, their receptors, and downstream intracellular targets MEK and ERK in the survival
347 biology of HGSOC cells in dormant culture and in vivo in xenografts. Furthermore, we reveal
348 that overexpression of Netrin-1 and -3 are correlated with poor clinical outcome in HGSOC and
349 over expression of these ligands induces elevated survival in dormant HGSOC culture conditions
350 and increased disease spread in a xenograft model of dissemination. Our work implicates
351 Netrins, their receptors, and MEK-ERK as a previously unappreciated, but critical signaling
352 network in HGSOC survival.

353 HGSOC spheroid cell biology has presented a unique challenge to cancer chemotherapy.
354 Dormant spheroids are most abundant in patients with late-stage disease and they contribute to
355 therapeutic resistance and seed metastases (39-41). Hence, there is a critical unmet need to
356 understand HGSOC spheroid dependencies and target them therapeutically. Our data suggests
357 that Netrin signaling is a universally active mechanism in spheroid cell survival. HGSOC is
358 characterized by extensive genomic rearrangements and copy number variants (38), and we
359 speculate that Netrin signaling is retained because of the extensive redundancy of components of
360 this pathway. Netrin-1 and -3 can both contribute to survival signaling and knock out of three or
361 four different Netrin receptors is necessary to compromise Netrin signaling in survival. A key
362 goal for the future is to identify Netrin-1 or -3 overexpression patients and compare their specific

363 disease progression patterns with our xenograft model. This will be most informative of the
364 effects of Netrin ligand overexpression in scenarios of dormancy, metastasis, and chemotherapy
365 resistance.

366 This study demonstrates that Netrins function to stimulate UNC5H and fibronectin repeat
367 containing receptors such as DCC to activate survival signals in HGSOC spheroids. This is
368 distinct from the known role of UNC5H and DCC as dependence receptors where Netrin inhibits
369 their pro-apoptotic signaling (25). Our data does not show elevated survival of spheroid cells in
370 response to deletions of receptors, even in instances where families of Netrin receptors are co-
371 deleted. Consistent with this observation, over expression of Netrin-1 or -3 in OVCAR8 cells
372 stimulates higher level survival in suspension. In colon cancer, deletion of DCC confers a
373 survival advantage and underscores the dependence receptor concept (42, 43). In HGSOC DCC
374 or UNC5H deletions are relatively rare (38). This suggests that ovarian cancer cells utilize Netrin
375 signals for positive survival signaling instead of to neutralize inherent death signals from
376 dependence receptors. Our data suggests that Netrin activates MEK and ERK to support cell
377 survival indicating that targeting ligands, receptors or downstream at MEK are all possible
378 approaches to inhibit this survival pathway. Netrin-1 inhibition in solid tumor xenograft models
379 of melanoma have been shown to be effective in combination with chemotherapy (44), but its
380 effects on a dormant scenario are unknown. Identifying agents that cooperate with standard
381 HGSOC chemotherapeutic agents such as carboplatin would offer an attractive strategy to
382 eradicate dormant cells while combating progressive disease. Alternatively, a novel approach to
383 targeting dormancy discovered in this study is, ironically, MEK inhibition. While MAPK
384 signaling in cancer is universally known for its role in proliferation (45), and MEK inhibitors are
385 used to block proliferation (46, 47), it is noteworthy that Netrin stimulation of MAPK signaling

386 is reported to provide survival signals and to guide axon outgrowth in a non-proliferative context
387 (26, 48). Dormancy is characterized by low phospho-ERK levels (3, 6), indicating low MEK
388 activity, however low levels of RAS-MAPK signaling are known to provide survival signals
389 (45). A challenge with deploying MEK inhibitors as an anti-dormancy setting in HGSOC therapy
390 is its incompatibility with standard chemotherapies that rely on cell proliferation. Overall, our
391 study aimed to identify potential new therapeutic targets in dormancy and Netrins and MEK are
392 potential new candidates for dormant HGSOC disease.

393 Current literature offers little to connect Netrins with HGSOC beyond the observation
394 that *NTN1* expression is increased in tumors compared to benign lesions (49). Similarly,
395 dormancy literature does not include a role for Netrins (3-6, 50). However, we expect that Netrin
396 signaling may play an unappreciated role in dormancy in other cancer disease site paradigms. As
397 stated in the introduction, dormancy is characterized by acquisition of stem like properties, EMT,
398 and in most paradigms it involves rare cells establishing themselves in perivascular or bone
399 marrow niches and Netrins have also been implicated in these processes (51-55). Inhibition of
400 Netrin-1 with NP137 and treatment with decitabine has been shown to reduce lung seeding
401 suggesting that Netrins are relevant in a metastatic scenario that may include dormant
402 intermediate steps in dissemination (56). Furthermore, Netrin signaling through UNC5B is
403 known to direct vascular branching (57). This suggests that Netrins are available in the
404 perivascular niche where dormant cells often reside. Lastly, Netrin-1 has been shown to be a
405 component of the bone marrow niche that suppresses hematopoietic stem cell proliferation (51).
406 While not a cancer dormancy scenario, it indicates that Netrins support some solitary dormant
407 cell properties and are expressed by resident cells in the appropriate dormant cell niches beyond

408 just HGSOC. For these reasons we expect Netrins will have a significant role in tumor dormancy

409 beyond ovarian cancer.

410 **Methods**

411 *Cell Lines and Engineering Cas9+ cells:* High-grade serous ovarian cancer (HGSOC) cell lines
412 OVCAR3, OVCAR4, OVCAR8, COV318, TOV1946 and iOvCa147 were used in this study.
413 The iOvCa147 cells have previously been characterized and reported (58). All cell lines were
414 verified by STR analysis. iOvCa147, OVCAR8, and TOV1946 cells were engineered to express
415 Cas9 using pLentiCas9-Blast and clones were isolated. High Cas9 editing efficiency was
416 determined by viability studies using sgRNAs targeting selected fitness genes (PSMD1, PSMD2,
417 EIF3D) and a non-targeting control (LacZ) as previously described (59).

418 *Lentiviral sgRNA library preparation:* HEK293T cells were transfected with the combined A
419 and B components of the GeCKO v2 whole genome library (123,411 sgRNAs in total) along
420 with plasmids encoding lentiviral packaging proteins (60). Media was collected 2-3 days later,
421 cells and debris were pelleted by centrifugation, and supernatant containing viral particles was
422 filtered through a 0.45 μM filter and stored at −80°C with 1.1 g/100 mL BSA.

423 *GO-CRISPR screens in iOvCa147, OVCAR8, and TOV1946 cells:* Cas9-positive and Cas9-
424 negative cells were separately transduced with lentiviruses at a multiplicity of infection of 0.3
425 and with a predicted library coverage of >1000-fold. Cells were selected in puromycin and
426 maintained in complete media (DMEM/F12 with 10% FBS, 1% pen-strep-glutamine), containing
427 puromycin in all following steps. More than 10^9 cells were collected and split into three groups
428 consisting of approximately 3.0×10^8 cells. Triplicate samples of 6.2×10^7 cells were saved for
429 sgRNA sequence quantitation (T_0). The remaining cells were seeded at 2.0×10^6 cells/mL in 20
430 x 10 cm ULA plates. Following 2 days of culture, media containing spheroids was transferred to
431 10 x 15 cm adherent tissue culture plates. The next day unattached spheroid cells were collected
432 and re-plated onto additional 15 cm plates. This process was repeated for a total of 5 days to

433 maximally capture viable cells. Attached cells were collected and pooled for DNA extraction
434 (T_f). Genomic DNA was extracted using the QIAmp DNA Blood Maxi Kit (Qiagen, #51194).
435 PCR amplification and barcoding performed as described (Hart paper, Cell, 2015) using
436 NEBNext Q5 Ultra mastermix (NEB, # MO544). PCR products were extracted from agarose
437 using a Monarch DNA Gel Extraction Kit (NEB, # T1020), quantitated and next generation
438 sequencing was performed using an Illumina NextSeq 75 cycle High Output kit on an Illumina
439 NextSeq platform.

440 *TRACS analysis:* The library reference file containing a list of all sgRNAs and their sequences
441 (CSV file), raw reads for the pooled sgRNA library (FASTQ files (L0) and raw reads (FASTQ
442 files) for all T_0 and T_f timepoints and replicates for Cas9-positive and Cas9-negative cells were
443 loaded into TRACS (https://github.com/developerpiru/TRACS)(61). TRACS then automatically
444 trimmed the reads using Cutadapt (v1.15), built a Bowtie2 (v2.3.4.1) index and aligned the reads
445 using Samtools (v1.7). TRACS used the MAGeCK read count function (v0.5.6) to generate read
446 counts and incremented all reads by 1 to prevent zero counts and division-by-zero errors. The
447 TRACS algorithm was then run using this read count file to determine the Library Enrichment
448 Score (ES), Initial ES, Final ES and the Enrichment Ratio (ER) for each gene. VisualizeTRACS
449 was used to generate graphs of Initial and Final ratios.

450 *Pathway enrichment analyses:* For GO-CRISPR screens and multi-omics comparisons, we used
451 the filtered list of genes obtained using TRACS and performed gene ontology and pathway
452 enrichment analysis using the ConsensusPathDB enrichment analysis test (Release 34
453 (15.01.2019), http://cpdb.molgen.mpg.de/) for top-ranked genes of interest. p_{adj} values and ER
454 values for each gene were used as inputs. The minimum required genes for enrichment was set to
455 45 and the FDR-corrected p_{adj} value cutoff was set to < 0.01. The Reactome pathway dataset was

456 used as the reference. For each identified pathway, ConsensusPathDB provides the number of
457 enriched genes and a q value (p_{adj}) for the enrichment. Bar plots were generated in R 3.6.2 using
458 these values to depict the significant pathways identified.

459 *Generating DYRK1A knockout cells:* A double cutting CRISPR/Cas9 approach with a pair of
460 sgRNAs (sgRNA A and B) was used to completely excise exon 2 (322 bp region) of *DYRK1A*
461 using a px458 vector (Addgene #48138) that was modified to express the full CMV promoter.
462 PCR primers that flank the targeted region of *DYRK1A* were used to verify deletion. Single-cell
463 clones were generated by liming dilutions and evaluated for DYRK1A status by PCR, western
464 blot, and sequencing. See Supplemental Table 1 for sgRNA and PCR primer sequences.

465 *DYRK1A IP kinase assay:* Whole cell lysates from adherent parental iOvCa147 cells and
466 *DYRK1A*$^{-/-}$ cells were extracted using complete RIPA buffer and incubated overnight with
467 DYRK1A antibody (Cell Signaling Technology anti-DYRK1A rabbit antibody #8765). Samples
468 were then washed with buffer and Dynabeads (Thermo Fisher Scientific Dynabeads Protein G
469 #10003D) were added for 2 hours. Samples were then washed with buffer and recombinant Tau
470 protein (Sigma recombinant Tau protein #T0576) and ATP (Sigma #A1852) were added and
471 samples were incubated for 30 minutes at 37°C. 5x SDS was then added and samples were
472 resolved by SDS-PAGE. Antibodies used for western blotting were phosphospecific Tau
473 antibody (Cell Signaling Technology phospho-Tau Ser-404 rabbit antibody #20194) and Tau
474 protein (Cell Signaling Technology anti-Tau rabbit antibody #46687).

475 *RNA preparation and RNA-sequencing:* Total RNA was collected from parental iOvCa147 cells
476 and *DYRK1A*$^{-/-}$ cells from 24-hour adherent or 6-hour spheroid conditions using the Monarch
477 Total RNA Miniprep Kit (NEB #T2010S) as described above. RNA was collected in three
478 replicates for each condition (adherent and spheroids). Samples were quantitated using Qubit 2.0

479 Fluorometer (Thermo Fisher Scientific) and quality control analysis using Agilent 2100
480 Bioanalyzer (Agilent Technologies #G2939BA) and RNA 6000 Nano Kit (Agilent Technologies
481 #5067-1511). Ribosomal RNA removal and library preparation was performed using ScriptSeq
482 Complete Gold Kit (Illumina #BEP1206). High-throughput sequencing was performed on an
483 Illumina NextSeq 500 platform (mid-output, 150-cycle kit).

484 *RNA-seq analyses:* Raw FASTQ data was downloaded from Illumina BaseSpace. Reads were
485 aligned using STAR 2.6.1a(62) to the human genome
486 (Homo_sapiens.GRCh38.dna.primary_assembly.fa; sjdbGTFfile:
487 Homo_sapiens.GRCh38.92.gtf) to generate read counts. DESeq2 was run with BEAVR(63) and
488 used to analyze read counts (settings: False discovery rate (FDR): 10%; drop genes with less
489 than 1 reads) to identify differentially expressed genes ($\log_2$ fold change > 1 for upregulated
490 genes; or $\log_2$ fold change < -1 for downregulated genes; $p_{adj} < 0.05$) for the following
491 comparisons: parental iOvCa147 adherent cells vs. parental iOvCa147 spheroid cells; or parental
492 iOvCa147 spheroid cells vs. *DYRK1A*$^{-/-}$ spheroid cells. For RNA-seq, we formed pathway
493 analyses in BEAVR and downloaded the pathway enrichment table to construct bar plots and
494 determine overlapping pathways using R 3.6.2.

495 *Western blots:* Adherent cells were washed in 1x PBS and lysed on the plate by the addition of
496 complete RIPA buffer with protease (Cell Signaling Technology #5871S) and phosphatase (Cell
497 Signaling Technologies #5870S) inhibitors and incubated for 5-10 minutes on ice. Spheres were
498 collected by gentle centrifugation at 300 rpm, washed gently in ice cold PBS, centrifuged again
499 and then resuspended in RIPA buffer as above. Samples were then centrifuged at 14,000 RPM at
500 4°C for 10 minutes. The supernatant liquid for each sample was collected and the pellets re-
501 extracted with RIPA containing the above inhibitor cocktails. Following centrifugation, the

502 supernatants for each treatment were collected and pooled. Protein was determined by Bradford
503 assay. To assess the effect of Netrin 1 on downstream signaling, spheres incubated under non
504 adherent conditions for 5 days were challenged with the addition of 500 ng/ml human
505 recombinant Netrin-1 (R&D Systems #6419-N1-025) for a period of 20 minutes before collection.
506 Lysates were mixed with 5x SDS loading dye buffer and resolved using standard SDS-PAGE
507 protocols. Antibodies used for blotting were p42/44 MAPK (Erk1/2) (Cell Signaling Technology
508 rabbit antibody #4695), Phospho-p44/42 MAPK(Erk1/2) T202/Y204 (Cell Signaling
509 Technology; rabbit antibody #4370), p38 MAPK (Cell Signaling Technology; rabbit antibody
510 #9212), p38 MAPK T180/Y182 (Cell Signaling Technology; rabbit antibody #9211),
511 p130(RBL2, Santa Cruz Biotechnology, rabbit antibody sc-317 discontinued), Ki67 (Abcam
512 rabbit antibody, # ab16667), DYRK1A (Cell Signaling Technology anti-DYRK1A rabbit
513 antibody #8765), Netrin-1 (Abcam rabbit antibody #ab126729), Netrin-3 (Abcam rabbit antibody
514 #ab185200), α-tubulin (Cell Signaling Technology anti-αTubulin rabbit antibody #2125) and β-
515 actin (Millipore Sigma rabbit antibody #A2066).

516 *RT-qPCR analysis of gene expression:* Cells from a minimum of three biological replicates were
517 triturated off the plate using Versene (0.5mM EDTA in PBS), collected, counted and 10^6 cells
518 plated onto Ultra-Low Attachment cell culture dishes (Corning) to induce sphere formation. The
519 spheres were collected after 24 h and RNA extracted using the Monarch Total RNA Miniprep
520 Kit (New England Biolabs #T2010S). RNA was extracted from adherent cells directly from the
521 plate. Extracted RNA was quantitated using a NanoDrop and stored at -80° until used. First
522 strand cDNA was generated from isolated RNA using the iScript cDNA Synthesis Kit (Bio-Rad,
523 #1708890) and RT-qPCR performed on the resulting cDNA (diluted 5-fold) using the iQ SYBR
524 Green Supermix (Bio-Rad, #1708882) and following the manufactures instructions. Reactions

525 were performed in 0.2ml non-skirted low profile 96 well PCR plates (Thermo Scientific, #AD-
526 0700) using a CFX Connect Real Time System thermo-cycler (Bio-Rad).

527 *TCGA patient data analyses:* We used the cBioPortal for Cancer Genomics
528 (https://www.cbioportal.org)(64) to analyze Netrin pathway alterations in Ovarian Serous
529 Cystadenocarcinoma patients (TCGA, PanCancer Atlas) for genomic alterations and mRNA
530 expression. OncoPrints were generated for mRNA expression (mean z-score threshold ± 1.5),
531 and mutations and putative copy number alterations for the following genes: *NTN1, NTN3,*
532 *NTN4, NTN5, UNC5A, UNC5B, UNC5C, UNC5D, DCC, DSCAM*. Survival analysis of *NTN1,*
533 and *-3* utilized patients from TCGA, PanCancer Atlas dataset and RNA-seq expression (high
534 expression z-score threshold > 1.2 and low is below 1.2).

535 *Generation of gene knockout cell lines:* Gibson Assembly (NEB #E2611) was used to clone
536 sgRNAs sequences derived from the GeCKO v2 library per gene of interest (*NTN1, NTN3,*
537 *NTN4, NTN5, DSCAM, DCC, NEO1, UNC5A, UNC5B, UNC5C, UNC5D,* and *EGFP* control
538 (See Supplemental Table 1 for sgRNA sequences for each)) into lentiCRISPR v2 (Addgene
539 #52961). For individual gene knockouts pooled libraries of up to four sgRNAs were generated.
540 For multiple gene knockouts pooled libraries of two sgRNAs/gene were constructed. To each 20-
541 nucleotide guide (Supplemental table I) was appended the 5' sequence, 5'-
542 TATCTTGTGGAAAGGACGAAACACC-3' and the 3' sequence, 5'-
543 GTTTTAGAGCTAGAAATAGCAAGTTAAAAT-3' (65). A 100 bp fragment was then
544 generated using the forward primer, 5'-
545 GGCTTTATATATCTTGTGGAAAGGACGAAACACCG-3', and reverse primer, 5'-
546 CTAGCCTTATTTTAACTTGCTATTTCTAGCTCTAAAAC-3′. The resulting gel purified
547 fragment was quantitated by Qubit and cloned into the lentiviral vector LentiCRISPR-V2

548 previously digested with BsmBI (New England Biolabs, # R0739) as described (65). To generate
549 virus particles, HEK293T cells were transfected with the assembled plasmid along with plasmids
550 encoding lentiviral packaging proteins. Media was collected after 2-3 days and any cells or
551 debris were pelleted by centrifugation at 500 x g. Supernatant containing viral particles was
552 filtered through a low protein binding 0.45 μM filter. For each knockout, it was important to
553 ensure that each target cell was transduced with a full complement of guides. To ensure this, the
554 cells were transduced at relatively high MOI. Briefly, 25,000 cells were plated and transduced
555 with fresh HEK293T conditioned media containing virus. While we did not titer the viral
556 preparations for these experiments, previous experience indicated that we could generate
557 sufficiently high virus titers using our protocol. Under these conditions, we found a lack of
558 puromycin sensitive cells following 2-3 days in media containing 2-4 μg/ml puromycin
559 indicating that every cell received at least one virus particle. Multi-gene knock outs were created
560 through multiple rounds of infection with the relevant culture supernatants followed by one
561 round of puromycin selection.

562 *Generation of gene overexpression cell lines:* Plasmids encoding Netrin1 and Netrin3 were
563 obtained from Addgene (Ntn1-Fc-His, #72104 and Ntn3-Fc-His, #72105). Netrin1 was PCR
564 amplified using the forward primer 5'-
565 GCTATCGATATCCCAAACGCCACCATGATGCGCGCTGTGTGGGAGGCGCTG-3' and
566 reverse 5'-GCTATCTCTAGAGGCCTTCTTGCACTTGCCCTTCTTCTCCCG-3' and cloned
567 into the EcoRV/XbaI sites of pcDNA3.1/myc-HisA. For lentiviral expression, pcDNA NTN1
568 was amplified using the primers, forward 5'-
569 CACTGTAGATCTCCAAACGCCACCATGATGCGCGCTGTGTGGGAGGCGCTG-3' and,
570 reverse 5'-ACGCGTGAATTCTTATCAACCGGTATGCATATTCAGATCCTCTTCTGAGAT-

571 3' while NTN3 was amplified from pcDNA NTN3 using, forward 5'-
572 CTCGAGAGATCTGCGGCCGCCACCATGCCTGGCTGGCCCTGG-3' and the same reverse
573 primer as for NTN1. In this way both constructs carry a C-terminal Myc tag. Both cDNA's were
574 inserted into the BamHI/EcoRI sites of the lentiviral expression vector FUtdTW (Addgene
575 #22478). Construction of lentiviral particle and transduction into the target cells was as described
576 above.

577 *Spheroid formation and reattachment viability assays:* For each targeted gene or cDNA
578 expressed in iOvCa147, OVCAR3, OVCAR4, OVCAR8, COV318, or TOV1946 cells, spheroid
579 viability was assayed as follows: Three to ten biological replicate cultures of knockout cells were
580 cultured for 72 hours in suspension conditions using ULA plasticware (2×10^6 cells per well) to
581 allow spheroid formation. Addition of therapeutics (Tramatinib, Selleckchem, #S4484) was
582 made at the time of plating. Spheroids were collected and transferred directly to standard
583 plasticware to facilitate reattachment for 24 hours, or dissociated and mixed with trypan blue.
584 Reattached cells were fixed in 25% methanol in PBS for 3 minutes. Fixed cells were incubated
585 for 30 minutes with shaking in 0.5% crystal violet, 25% methanol in PBS. Plates were carefully
586 immersed in water to remove residual crystal violet and destained in 10% acetic acid in 1x PBS
587 for 1 hour with shaking to extract crystal violet from cells. Absorbance of crystal violet was
588 measured at 590 nm using a microplate reader (Perkin Elmer Wallac 1420).

589 *Xenografts:* All animal experiments were approved by the Animal Care Committee at Western
590 University (protocol #2020-039). ARRIVE principles were followed in carrying out xenograft
591 experiments. Female NOD-SCID mice were purchased from JAX (#001303). They were
592 randomly selected prior to being engrafted between six and eight weeks of age with 4 $x10^6$
593 OVCAR8 control or modified derivatives. Five to ten mice were housed for 14 days, 35 days, or

594 until humane endpoint for each OVCAR8 or modified derivative. Following euthanasia all mice
595 were subjected to a necropsy to analyze disease spread. Tumor lesions were photographed and
596 quantitated by individuals unaware of the genotypes. Abdominal organs and associated tumor
597 lesions were fixed in 10% formalin overnight and transferred to 70% ethanol and later
598 embedded, sectioned and stained as described below. In cases where abdominal washes were
599 performed, an incision was made in the peritoneal membrane and PBS was injected, the
600 abdominal region was agitated and PBS was withdrawn using a P1000 pipet tip and aliquoted for
601 downstream analysis in cell culture and qPCR.

602 *Patient derived spheroids:* Patient derived spheroids were isolated from ascites fluid obtained
603 from debulking surgical procedures. These HGSOC samples were obtained with permission and
604 institutional research ethics oversight (Project ID #115904). Spheroids were prepared by filtering
605 the ascites fluid through a 100μm mesh filter and washing the captured spheroids from the filter
606 with PBS. The spheres were collected by gravity on ice in PBS, washed twice with ice cold PBS
607 and allowed to settle on ice. Spheres were then fixed for 20 minutes in 10% formalin, washed,
608 and resuspended in PBS before being embedded in paraffin.

609 *Histology and immunohistochemistry:* Fixed organs from xenografts or spheroids were
610 embedded in paraffin, sectioned, and stained with H&E using standard methods. For
611 immunohistochemistry, sections were deparaffinized by standard procedures and antigen
612 retrieval was performed in 10mM citrate, pH6.0. The sections were blocked with 10% goat
613 serum/3% BSA/0.3% Triton X-100 and stained with antibodies to Netrin-1 (Abcam #ab126729,
614 1:200), Cytokeratin (human specific cytokeratin 7 and 8, ZETA Corporation #Z2018ML, 1:200),
615 EpCAM (Cell Signaling Technology, #14452, 1:250), p53 (Cell Signaling Technologies, #2527,
616 1:125), Netrin-3 (1:250), Ki67 (Cell Signaling Technology, #12202, 1:400) and p130 (RBL2,

617 Santa Cruz Biotechnology, SC-317, 1:150). Netrin-3 antibodies were generated using immunized
618 rabbits and their generation and purification will be published elsewhere. Primary antibodies
619 were followed with a biotinylated anti-rabbit (Vector Labs, # BA-1000) or anti-mouse (Jackson
620 ImmunoResearch, #115-067-003) IgG as a secondary antibody (1:500). Proteins were visualized
621 using DAB chemistry (ImmPACT DAB, Vector Labs, #SK-4105).

622 *Statistical analyses:* Specific statistical tests used are indicated in the figure legends for each
623 experiment. Analysis was done using GraphPad Prism 6.

624

625

626 **Materials availability**

627 All previously unpublished reagents created in this study are available on request from the
628 corresponding author.

629

630 **Data availability**

631 All sequencing data have been deposited in GEO under accession codes GSE190294 and
632 GSE150246. Source data for graphs and original blots are available in source data files, or from
633 public databases as described in the methods section.

634 **References**

635 1. Giancotti FG. Mechanisms governing metastatic dormancy and reactivation. Cell.
636 2013;155(4):750-64.
637 2. Massague J, Ganesh K. Metastasis-Initiating Cells and Ecosystems. Cancer Discov.
638 2021;11(4):971-94.
639 3. Sosa MS, Bragado P, Aguirre-Ghiso JA. Mechanisms of disseminated cancer cell
640 dormancy: an awakening field. Nat Rev Cancer. 2014;14(9):611-22.
641 4. Phan TG, Croucher PI. The dormant cancer cell life cycle. Nat Rev Cancer.
642 2020;20(7):398-411.
643 5. Goddard ET, Bozic I, Riddell SR, Ghajar CM. Dormant tumour cells, their niches and the
644 influence of immunity. Nat Cell Biol. 2018;20(11):1240-9.
645 6. Yeh AC, Ramaswamy S. Mechanisms of Cancer Cell Dormancy--Another Hallmark of
646 Cancer? Cancer Res. 2015;75(23):5014-22.
647 7. Correa RJ, Peart T, Valdes YR, DiMattia GE, Shepherd TG. Modulation of AKT activity
648 is associated with reversible dormancy in ascites-derived epithelial ovarian cancer spheroids.
649 Carcinogenesis. 2012;33(1):49-58.
650 8. Lengyel E, Burdette JE, Kenny HA, Matei D, Pilrose J, Haluska P, et al. Epithelial
651 ovarian cancer experimental models. Oncogene. 2014;33(28):3619-33.
652 9. Hu J, Nakhla H, Friedman E. Transient arrest in a quiescent state allows ovarian cancer
653 cells to survive suboptimal growth conditions and is mediated by both Mirk/dyrk1b and
654 p130/RB2. Int J Cancer. 2011;129(2):307-18.
655 10. MacDonald J, Ramos-Valdes Y, Perampalam P, Litovchick L, DiMattia GE, Dick FA. A
656 Systematic Analysis of Negative Growth Control Implicates the DREAM Complex in Cancer
657 Cell Dormancy. Mol Cancer Res. 2017;15(4):371-81.
658 11. Correa RJ, Valdes YR, Peart TM, Fazio EN, Bertrand M, McGee J, et al. Combination of
659 AKT inhibition with autophagy blockade effectively reduces ascites-derived ovarian cancer cell
660 viability. Carcinogenesis. 2014;35(9):1951-61.
661 12. Correa RJ, Valdes YR, Shepherd TG, DiMattia GE. Beclin-1 expression is retained in
662 high-grade serous ovarian cancer yet is not essential for autophagy induction in vitro. J Ovarian
663 Res. 2015;8:52.
664 13. Shepherd TG, Dick FA. Principles of dormancy evident in high-grade serous ovarian
665 cancer. Cell Div. 2022;17(1):2.
666 14. Lheureux S, Gourley C, Vergote I, Oza AM. Epithelial ovarian cancer. Lancet.
667 2019;393(10177):1240-53.
668 15. Lengyel E. Ovarian cancer development and metastasis. Am J Pathol. 2010;177(3):1053-
669 64.
670 16. Bowtell DD, Bohm S, Ahmed AA, Aspuria PJ, Bast RC, Jr., Beral V, et al. Rethinking
671 ovarian cancer II: reducing mortality from high-grade serous ovarian cancer. Nat Rev Cancer.
672 2015;15(11):668-79.
673 17. Peart T, Ramos Valdes Y, Correa RJ, Fazio E, Bertrand M, McGee J, et al. Intact LKB1
674 activity is required for survival of dormant ovarian cancer spheroids. Oncotarget.
675 2015;6(26):22424-38.
676 18. Buensuceso A, Ramos-Valdes Y, DiMattia GE, Shepherd TG. AMPK-Independent
677 LKB1 Activity Is Required for Efficient Epithelial Ovarian Cancer Metastasis. Mol Cancer Res.
678 2019.

679 19. Chen MW, Yang ST, Chien MH, Hua KT, Wu CJ, Hsiao SM, et al. The STAT3-miRNA-
680 92-Wnt Signaling Pathway Regulates Spheroid Formation and Malignant Progression in Ovarian
681 Cancer. Cancer Res. 2017;77(8):1955-67.
682 20. Diaz Osterman CJ, Ozmadenci D, Kleinschmidt EG, Taylor KN, Barrie AM, Jiang S, et
683 al. FAK activity sustains intrinsic and acquired ovarian cancer resistance to platinum
684 chemotherapy. Elife. 2019;8.
685 21. Rajasekharan S, Kennedy TE. The netrin protein family. Genome Biol. 2009;10(9):239.
686 22. Kryza D, Wischhusen J, Richaud M, Hervieu M, Sidi Boumedine J, Delcros JG, et al.
687 From netrin-1-targeted SPECT/CT to internal radiotherapy for management of advanced solid
688 tumors. EMBO Mol Med. 2023;15(4):e16732.
689 23. Mehlen P, Delloye-Bourgeois C, Chedotal A. Novel roles for Slits and netrins: axon
690 guidance cues as anticancer targets? Nat Rev Cancer. 2011;11(3):188-97.
691 24. Arakawa H. Netrin-1 and its receptors in tumorigenesis. Nat Rev Cancer.
692 2004;4(12):978-87.
693 25. Brisset M, Grandin M, Bernet A, Mehlen P, Hollande F. Dependence receptors: new
694 targets for cancer therapy. EMBO Mol Med. 2021;13(11):e14495.
695 26. Forcet C, Stein E, Pays L, Corset V, Llambi F, Tessier-Lavigne M, et al. Netrin-1-
696 mediated axon outgrowth requires deleted in colorectal cancer-dependent MAPK activation.
697 Nature. 2002;417(6887):443-7.
698 27. Larrieu-Lahargue F, Welm AL, Thomas KR, Li DY. Netrin-4 induces lymphangiogenesis
699 in vivo. Blood. 2010;115(26):5418-26.
700 28. Yin K, Wang L, Zhang X, He Z, Xia Y, Xu J, et al. Netrin-1 promotes gastric cancer cell
701 proliferation and invasion via the receptor neogenin through PI3K/AKT signaling pathway.
702 Oncotarget. 2017;8(31):51177-89.
703 29. Llambi F, Lourenco FC, Gozuacik D, Guix C, Pays L, Del Rio G, et al. The dependence
704 receptor UNC5H2 mediates apoptosis through DAP-kinase. EMBO J. 2005;24(6):1192-201.
705 30. Castets M, Coissieux MM, Delloye-Bourgeois C, Bernard L, Delcros JG, Bernet A, et al.
706 Inhibition of endothelial cell apoptosis by netrin-1 during angiogenesis. Dev Cell.
707 2009;16(4):614-20.
708 31. Bruikman CS, Zhang H, Kemper AM, van Gils JM. Netrin Family: Role for Protein
709 Isoforms in Cancer. J Nucleic Acids. 2019;2019:3947123.
710 32. Jiang S, Richaud M, Vieugue P, Rama N, Delcros JG, Siouda M, et al. Targeting netrin-3
711 in small cell lung cancer and neuroblastoma. EMBO Mol Med. 2021;13(4):e12878.
712 33. Shepherd TG, Theriault BL, Campbell EJ, Nachtigal MW. Primary culture of ovarian
713 surface epithelial cells and ascites-derived ovarian cancer cells from patients. Nat Protoc.
714 2006;1(6):2643-9.
715 34. Litovchick L, Chestukhin A, DeCaprio JA. Glycogen synthase kinase 3 phosphorylates
716 RBL2/p130 during quiescence. Molecular and cellular biology. 2004;24(20):8970-80.
717 35. Zanoni M, Piccinini F, Arienti C, Zamagni A, Santi S, Polico R, et al. 3D tumor spheroid
718 models for in vitro therapeutic screening: a systematic approach to enhance the biological
719 relevance of data obtained. Sci Rep. 2016;6:19103.
720 36. Di Vona C, Bezdan D, Islam AB, Salichs E, Lopez-Bigas N, Ossowski S, et al.
721 Chromatin-wide profiling of DYRK1A reveals a role as a gene-specific RNA polymerase II
722 CTD kinase. Mol Cell. 2015;57(3):506-20.
723 37. Meijers R, Smock RG, Zhang Y, Wang JH. Netrin Synergizes Signaling and Adhesion
724 through DCC. Trends Biochem Sci. 2020;45(1):6-12.

725 38. Network CGA. Integrated genomic analyses of ovarian carcinoma. Nature.
726 2011;474(7353):609-15.
727 39. Ahmed N, Stenvers KL. Getting to know ovarian cancer ascites: opportunities for
728 targeted therapy-based translational research. Front Oncol. 2013;3:256.
729 40. Narod S. Can advanced-stage ovarian cancer be cured? Nat Rev Clin Oncol.
730 2016;13(4):255-61.
731 41. Keyvani V, Farshchian M, Esmaeili SA, Yari H, Moghbeli M, Nezhad SK, et al. Ovarian
732 cancer stem cells and targeted therapy. J Ovarian Res. 2019;12(1):120.
733 42. Fearon ER, Cho KR, Nigro JM, Kern SE, Simons JW, Ruppert JM, et al. Identification of
734 a chromosome 18q gene that is altered in colorectal cancers. Science. 1990;247(4938):49-56.
735 43. Mehlen P, Rabizadeh S, Snipas SJ, Assa-Munt N, Salvesen GS, Bredesen DE. The DCC
736 gene product induces apoptosis by a mechanism requiring receptor proteolysis. Nature.
737 1998;395(6704):801-4.
738 44. Boussouar A, Tortereau A, Manceau A, Paradisi A, Gadot N, Vial J, et al. Netrin-1 and
739 Its Receptor DCC Are Causally Implicated in Melanoma Progression. Cancer Res.
740 2020;80(4):747-56.
741 45. Downward J. Targeting RAS signalling pathways in cancer therapy. Nat Rev Cancer.
742 2003;3(1):11-22.
743 46. Barbosa R, Acevedo LA, Marmorstein R. The MEK/ERK Network as a Therapeutic
744 Target in Human Cancer. Mol Cancer Res. 2021;19(3):361-74.
745 47. Flaherty KT, Infante JR, Daud A, Gonzalez R, Kefford RF, Sosman J, et al. Combined
746 BRAF and MEK inhibition in melanoma with BRAF V600 mutations. N Engl J Med.
747 2012;367(18):1694-703.
748 48. Chen J, Du H, Zhang Y, Chen H, Zheng M, Lin P, et al. Netrin-1 Prevents Rat Primary
749 Cortical Neurons from Apoptosis via the DCC/ERK Pathway. Front Cell Neurosci. 2017;11:387.
750 49. Papanastasiou AD, Pampalakis G, Katsaros D, Sotiropoulou G. Netrin-1 overexpression
751 is predictive of ovarian malignancies. Oncotarget. 2011;2(5):363-7.
752 50. Recasens A, Munoz L. Targeting Cancer Cell Dormancy. Trends Pharmacol Sci.
753 2019;40(2):128-41.
754 51. Renders S, Svendsen AF, Panten J, Rama N, Maryanovich M, Sommerkamp P, et al.
755 Niche derived netrin-1 regulates hematopoietic stem cell dormancy via its receptor neogenin-1.
756 Nat Commun. 2021;12(1):608.
757 52. Ozmadenci D, Feraud O, Markossian S, Kress E, Ducarouge B, Gibert B, et al. Netrin-1
758 regulates somatic cell reprogramming and pluripotency maintenance. Nat Commun.
759 2015;6:7398.
760 53. Lengrand J, Pastushenko I, Vanuytven S, Song Y, Venet D, Sarate RM, et al.
761 Pharmacological targeting of netrin-1 inhibits EMT in cancer. Nature. 2023;620(7973):402-8.
762 54. Ducarouge B, Redavid AR, Victoor C, Chira R, Fonseca A, Hervieu M, et al. Netrin-1
763 blockade inhibits tumor associated Myeloid-derived suppressor cells, cancer stemness and
764 alleviates resistance to chemotherapy and immune checkpoint inhibitor. Cell Death Differ. 2023.
765 55. Cassier PA, Navaridas R, Bellina M, Rama N, Ducarouge B, Hernandez-Vargas H, et al.
766 Netrin-1 blockade inhibits tumour growth and EMT features in endometrial cancer. Nature.
767 2023;620(7973):409-16.
768 56. Grandin M, Meier M, Delcros JG, Nikodemus D, Reuten R, Patel TR, et al. Structural
769 Decoding of the Netrin-1/UNC5 Interaction and its Therapeutical Implications in Cancers.
770 Cancer Cell. 2016;29(2):173-85.

771 57. Lu X, Le Noble F, Yuan L, Jiang Q, De Lafarge B, Sugiyama D, et al. The netrin
772 receptor UNC5B mediates guidance events controlling morphogenesis of the vascular system.
773 Nature. 2004;432(7014):179-86.
774 58. Tong JG, Valdes YR, Sivapragasam M, Barrett JW, Bell JC, Stojdl D, et al. Spatial and
775 temporal epithelial ovarian cancer cell heterogeneity impacts Maraba virus oncolytic potential.
776 BMC Cancer. 2017;17(1):594.
777 59. Hart T, Chandrashekhar M, Aregger M, Steinhart Z, Brown KR, MacLeod G, et al. High-
778 Resolution CRISPR Screens Reveal Fitness Genes and Genotype-Specific Cancer Liabilities.
779 Cell. 2015;163(6):1515-26.
780 60. Sanjana NE, Shalem O, Zhang F. Improved vectors and genome-wide libraries for
781 CRISPR screening. Nat Methods. 2014;11(8):783-4.
782 61. Perampalam P, MacDonald JI, Dick FA. GO-CRISPR; a highly controlled workflow to
783 discover gene essentiality. bioRxiv. 2020;doi: https://doi.org/10.1101/2020.06.04.134841.
784 62. Dobin A, Davis CA, Schlesinger F, Drenkow J, Zaleski C, Jha S, et al. STAR: ultrafast
785 universal RNA-seq aligner. Bioinformatics. 2013;29(1):15-21.
786 63. Perampalam P, Dick FA. BEAVR: a browser-based tool for the exploration and
787 visualization of RNA-seq data. BMC Bioinformatics. 2020;21(1):221.
788 64. Cerami E, Gao J, Dogrusoz U, Gross BE, Sumer SO, Aksoy BA, et al. The cBio cancer
789 genomics portal: an open platform for exploring multidimensional cancer genomics data. Cancer
790 Discov. 2012;2(5):401-4.
791 65. Wang T, Lander ES, Sabatini DM. Large-Scale Single Guide RNA Library Construction
792 and Use for CRISPR-Cas9-Based Genetic Screens. Cold Spring Harb Protoc. 2016;2016(3):pdb
793 top086892.

794

795 **Figure Legends**

796 **Figure 1. GO-CRISPR screens implicate axon guidance pathways as supporting HGSOC**
797 **spheroid cell viability. A)** iOvCa147, TOV1946, or OVCAR8 cells were cultured under
798 adherent conditions (Adh) or in suspension to induce spheroid formation (Sph). Lysates were
799 prepared and analyzed by western blotting for the proliferation marker Ki67 and the quiescence
800 marker p130, and phosphorylated and total levels of ERK and p38. Tubulin was blotted as a
801 loading control. **B)** Flow chart of GO-CRISPR screening used for each of iOvCa147, TOV1946,
802 or OVCAR8 control cells and derivatives of each that express Cas9. Cas9-positive cells (top
803 row) and Cas9-negative cells (bottom row) were transduced with the GeCKO v2 pooled sgRNA
804 library. After antibiotic selection, cells were expanded under adherent culture conditions (0
805 hours) before being transferred to suspension culture conditions to induce spheroid formation
806 and select for cell survival. After 48 hours spheroids were transferred to standard plasticware to
807 isolate viable cells. Red arrows indicate the relevant comparisons of sgRNA sequence abundance
808 that were made to analyze screen outcomes. Genes with relatively greater effect on viability in
809 suspension were selected by comparing their scores between adherent and suspension conditions
810 and considering genes with an enrichment ratio (ER) of <1. **C)** Scatter plots representing the
811 spheroid score on y-axis and adherent score on the x-axis calculated by TRACS for each gene in
812 each cell line (iOvCa147, TOV1946, OVCAR8). Colored data points represent genes with ER <
813 1 and $p_{adj} < 0.05$ (paired t-test). **D)** Venn diagram illustrating overlap of genes identified as
814 supporting cell viability in suspension culture from iOvCa147, TOV1946, and OVCAR8 cells.
815 **E)** Graph depicting enriched pathways from ConsensusPathDB using the 1382 commonly
816 identified genes from D. Categories are ranked by q-value. Tiers of Reactome categories are
817 indicated by shading.

818 **Figure 1 - Figure Supplement 1. CRISPR screen analysis details and internal controls. A)**
819 Flowchart of data analysis used to identify genes that are most relevant to ovarian cancer cell
820 survival in suspension. **B)** Mathematical formulas to define gene scores, enrichment scores
821 (n=guides per gene), and enrichment ratios used by TRACS. **C)** Reader-operator curves were
822 generated to assess TRACS categorization of 1000 non-targeting control sgRNAs in the
823 GeCKOv2 library for each of the three cell lines screened. **D)** Spheroid cell viability levels from
824 low throughput siRNA gene knock downs for 35 genes in iOvCa147 and OVCAR8 cells was
825 plotted against the enrichment ratio for the same genes in the same two cell lines from this
826 screen. These independent approaches to measure viability were compared using linear
827 regression.

828

829 **Figure 2. Axon guidance pathway components are upregulated in iOvCa147 spheroid cells**
830 **in a DYRK1A dependent manner. A)** RNA was isolated from iOvCa147 cells following
831 culture under adherent conditions or in suspension conditions to induce spheroid formation for 6
832 hours. Triplicate independent cultures were processed for RNA-seq. A volcano plot shows
833 differentially expressed genes in spheroid cells compared to adherent. 1,937 genes were found to
834 be downregulated in iOvCa147 spheroid cells ($\log_2$ fold change < 1, $p_{adj} < 0.05$ (Wald test), FDR
835 10%, highlighted in grey) and 1,834 genes were upregulated ($\log_2$ fold change > 1, $p_{adj} < 0.05$,
836 FDR 10%, highlighted in blue). **B)** Top 15 most significantly enriched pathways ($p_{adj} < 0.05$)
837 whose genes were upregulated in suspension culture compared to adherent in RNA-seq analysis.
838 **C)** A volcano plot showing differentially expressed genes in *DYRK1A*$^{-/-}$ spheroid cells compared

839 to iOvCa147 spheroid cells. 744 genes were found to be downregulated in *DYRK1A*$^{-/-}$ spheroid
840 cells ($\log_2$ fold change < 1, p_{adj} < 0.05 (Wald test), FDR 10%, highlighted in red) and 96 genes
841 were upregulated ($\log_2$ fold change > 1, p_{adj} < 0.05 (Wald test), FDR 10%, highlighted in grey).
842 **D)** Top 15 most significantly enriched pathways that were represented by downregulated genes
843 in *DYRK1A*$^{-/-}$ suspension culture compared to control cells in suspension. **E)** Venn diagram
844 depicting overlapping enriched pathways identified in GO-CRISPR screens in green; enriched
845 pathways identified in upregulated genes in parental iOvCa147 spheroid cells in blue; and
846 enriched pathways identified in downregulated genes in *DYRK1A*$^{-/-}$ spheroid cells in red. 78
847 pathways were commonly enriched in all three datasets (shown in yellow). **F)** Top 10 most
848 significantly enriched pathways among the 78 identified in C.

849 **Figure 2 - Figure Supplement 1. Generation of iOvCa147 cells deficient for DYRK1A and**
850 **loss of viability in suspension. A)** Strategy to generate *DYRK1A*$^{-/-}$ cells using a pair of sgRNAs
851 that flank exon 2. PCR For and PCR Rev primers flank exon 2 and are used to detect deletion
852 events. **B)** Agarose gel showing PCR products for iOVCA147 cells and putative *DYRK1A*$^{-/-}$
853 cells. The full length amplicon containing exon 2 was detected in parental iOvCa147 cells (1,348
854 bp). A smaller amplicon (1,026 bp) was detected in *DYRK1A*$^{-/-}$ cells, indicting successful
855 excision of the 322 bp region encompassing exon 2. **C)** Western blot comparing DYRK1A
856 expression in iOVCA147 cells and *DYRK1A*$^{-/-}$ cells. **D)** IP kinase assay to evaluate DYRK1A
857 activity in *DYRK1A*$^{-/-}$ cells. Anti-DYRK1A antibodies or IgG was used to immunoprecipitate
858 from iOVCA147 and *DYRK1A*$^{-/-}$ cells. Precipitates were incubated with ATP and Tau protein.
859 Samples were resolved by SDS-PAGE and probed with pSer404-Tau antibody. **E)** Parental
860 iOvCa147 or *DYRK1A*$^{-/-}$ cells were incubated in suspension conditions for 24 hours, 72 hours, or
861 4 days to induce spheroid formation, and then re-plated in adherent conditions for 24 hours to
862 allow reattachment. Reattached spheroid cells were stained with crystal violet and absorbance
863 was quantified. Alternatively, cells in suspension were isolated and utilized for Cell TitreGLO
864 cell viability measurements. *DYRK1A*$^{-/-}$ spheroid cells had impaired survival compared to
865 parental iOvCa147 spheroid cells at each time point and reattached and crystal violet stained cell
866 viability matched Cell TitreGLO measurements of viability (one way anova, ****P<0.0001).

867

868 **Figure 3. Expression of Netrin ligands and their dependence receptors is increased in**
869 **suspension culture. A-C)** RT-qPCR was performed to quantitate mRNA expression levels of
870 Netrin ligands and receptors in three different HGSOC cell lines. Relative expression of the
871 indicated transcripts is shown for suspension culture conditions compared with adherent. All
872 experiments were performed in at least triplicate biological replicates. Means were compared
873 with the same gene in adherent culture using a one way anova (*P<0.05, ****P<0.0001).

874

875 **Figure 4. Netrins are expressed in dormant patient derived spheroids.** Spheroids were
876 isolated from ascites of HGSOC patients and processed for immunohistochemical staining. **A-B)**
877 Serial sections from solid HGSOC tumors were stained with antibodies to p130, Ki67, or a no
878 primary antibody control (NP). Scale bar = 100µm for upper panels and 2mm for lower panels.
879 **C-E)** Serial spheroid sections from the indicated patients were stained with Ki67 and p130.

880 Sections with dense positive nuclear staining are indicated with white arrows. Scale bar =
881 100μm. **F-H)**. Immunohistochemical staining was performed for the indicated proteins on serial
882 sections of ascites derived spheroids. Omission of primary antibody was used a control for
883 background staining for each patient sample (NP). Scale bar = 100μm

884 **Figure 4 - Figure Supplement 1. Specificity of Netrin-1 and Netrin-3 IHC staining of**
885 **OVCAR8 spheroids. A)** OVCAR8 cells were allowed to form spheroids for six hours before
886 fixation in formalin and embedding in paraffin for sectioning. Serial sections were stained with
887 Netrin-1 Abs or a no primary antibody control. **B)** OVCAR8 cells overexpressing Netrin-1 were
888 used to prepare spheroids as in A and stained in parallel to samples in A. **C)** OVCAR8 deleted
889 for Netrin-1 expression were used to prepare spheroids as in A and serial sections were stained
890 for Netrin-1 or with a no primary antibody control and counter stained. **D)** OVCAR8 cells were
891 allowed to form spheroids for six hours before fixation in formalin and embedding in paraffin for
892 sectioning. Serial sections were stained with Netrin-3 Abs or a no primary antibody control. **E)**
893 OVCAR8 cells overexpressing Netrin-3 were used to prepare spheroids as in D and stained in
894 parallel to samples in D. **F)** OVCAR8 deleted for Netrin-3 expression were used to prepare
895 spheroids as in D and serial sections were stained for Netrin-3 or with a no primary antibody
896 control. All scale bars = 100μm

897

898 **Figure 5. Netrin ligands and their receptors are required for spheroid cell survival. A)**
899 Illustration of netrin ligands, receptors, and other intracellular signaling molecules that are
900 included in the Axon Guidance pathway category. The frequency of their identification in
901 CRISPR screens is illustrated by shading and indicates how many cell lines had an enrichment
902 ratio <1 for a given component. **B)** The indicated ovarian cancer cell lines were infected with
903 lentiviruses expressing sgRNAs directed against the indicated Netrin signaling genes. Cells were
904 transferred to suspension culture conditions to induce spheroid formation for 72 hours and then
905 returned to adherent conditions for 24 hours to facilitate reattachment. Re-attached cells were
906 stained with Crystal Violet and retained dye was extracted and quantitated to measure relative
907 survival. Each cell-gene combination was assayed in at least three biological replicates,
908 averaged, and viability is displayed as a bubble plot. Mean survival for a given cell-gene
909 combination was compared with GFP control gRNA transduced cells using one way anova and
910 significance levels are illustrated by bubble size. Inviable cell-gene combinations are depicted as
911 empty spaces. **C)** Cultures of the indicated cell lines were cultured in suspension for five days
912 and stimulated with 0.5 μg/mL Netrin-1. Netrin-1 signaling was analyzed by SDS-PAGE and
913 western blotting for phospho-ERK, ERK, and tubulin. **D)** Quiescent adherent OVCAR8 cells
914 were stimulated with 0.5 μg/mL Netrin-1 or 0.5 μg/mL EGF, and compared with OVCAR8 cells
915 in suspension stimulated as in C. Extracts were prepared and blotted for phospho-ERK, ERK,
916 and tubulin. **E)** Suspension cultures of OVCAR8, or knock out derivatives, were harvested and
917 analyzed for relative phosphorylation levels of ERK by western blotting. Total ERK and tubulin
918 blotting serve as expression and loading controls. **F)** Netrin-1 signaling in OVCAR8, UNC5
919 4KO and DDN 3KO derivatives was tested by transferring cells to suspension and stimulating
920 with Netrin-1 as before. Western blotting for phospho-ERK, ERK were also as before. **G)**

921 OVCAR8 cells were seeded in suspension culture and treated with the MEK inhibitors
922 PD184352, Trametinib or DMSO vehicle for 72 hours. Mean viability was determined by re-
923 attachment and compared by one way anova (****P<0.0001). **H)** OVCAR8 cells were cultured
924 in suspension and treated with Trametinib or DMSO vehicle as in G. Viability was determined
925 by trypan blue dye exclusion and compared by one way anova (**P<0.01). **I)** Extracts were
926 prepared from Trametinib and control treated spheroid cells and blotted for phospho-ERK, ERK,
927 and tubulin. **J)** Model summarizing the roles of Netrin ligands, receptors, and downstream
928 targets MEK and ERK in dormant survival signaling.

929 **Figure 5 - Figure Supplement 1. Evaluation of target gene transcript levels in multigene**
930 **knock out cells. A)** RT-qPCR was performed on RNA isolated from control sgRNA expressing
931 OVCAR8 cells and UNC5 4KO to assess expression of UNC5 family members. Graphs depict
932 relative expression levels for each indicted gene in control and knock out cell lines. Mean
933 expression levels of targeted cells were compared to background measurements using one way
934 anova (****P<0.0001). **B)** RT-qPCR was used to measure mRNA levels of NTN1 and NTN3
935 transcripts in their respective CRISPR targeted, and OVCAR8 controls. Mean values were
936 compared by one way anova (****P<0.0001). **C)** Levels of mRNA corresponding to DCC,
937 DSCAM, and NEO1 were determined by RT-qPCR in DDN 3KO cells and control OVCAR8.
938 Mean values were compared by one way anova (****P<0.0001). **D)** The indicated genotypes of
939 cells were subjected to suspension culture and protein extracts were prepared at the indicated
940 times. Proteins were resolved by SDS-PAGE, blotted, and probed with the indicated antibodies.

941

942 **Figure 6. Loss of Netrin signaling reduces spheroids and prolongs survival. A)** Control
943 OVCAR8L (negative control CRISPR targeted cells) and UNC5 4KO cells were injected into the
944 peritoneal space of female NOD/SCID mice. After two weeks, animals were euthanized and
945 engrafted cells were collected with abdominal washes. **B)** RT-qPCR was used to compare gene
946 expression of the indicated cell cycle markers in RNA extracted from proliferating cells in
947 culture before engraftment and compared with RNA obtained from spheroids in xenografted
948 mice. Technical replicates of RNA derived from three different mice is shown. **C)** Spheroids
949 obtained from abdominal washes from each mouse were plated in adherent conditions to
950 compare their abundance between control and UNC5 4KO genotypes. One example of each
951 genotype of cell is shown. Crystal violet staining and dye extraction were used to quantitate
952 biomass and averages were compared by one way anova (n=6, *P<0.05). **D)** DNA was extracted
953 from cells collected in abdominal washes and human Alu repeats were detected by qPCR to
954 quantitate and compare human cancer cells. Means were compared by one way anova (n=6,
955 **P<0.01). **E)** Control OVCAR8 and UNC5 4KO cells were xenografted as above and mice
956 were monitored until humane endpoint. **F)** Kaplan-Meier analysis of survival for mice engrafted
957 with the indicated genotypes of cells. Survival was compared by logrank test.

958 **Figure 6 - Figure Supplement 1. Evaluation of dormancy arrest in cell culture by RT-**
959 **qPCR.** RNA was extracted from asynchronously proliferating cells and suspension cultures 72
960 hours post transfer from adherent. RT-qPCR was used to compare gene expression of the
961 indicated cell cycle markers in iOvCa147, OVCAR8, TOV1946.

962

963 **Figure 7. Netrin ligand overexpression is associated with poor clinical outcome in HGSOC.**
964 **A)** TCGA RNA-seq data for HGSOC patients (TCGA PanCancer Atlas study) was used to
965 identify high Netrin-1 or -3 and low Netrin-1 or -3 expressing patients (high expressing are
966 above z-score 1.2). Overall survival was used to construct Kaplan-Meier plots and survival was
967 compared using a logrank test. **B)** OVCAR8 cells were stably transduced with lentiviral
968 constructs to overexpress epitope tagged Netrin-1 or -3. Western blotting for Netrins, Myc-tags,
969 and Actin were used to determine relative expression levels of both Netrins in these cell
970 populations and vector controls. **C)** Control and Netrin overexpressing cells were transferred to
971 suspension culture conditions to form spheroids, and replated to assay for viability. Mean
972 viability and standard deviation is shown for each. One way anova was used to compare survival
973 (* $P<0.05$, *** $P<0.001$). **D)** Reattached spheroids were fixed and stained with Crystal Violet to
974 examine size and abundance in control and Netrin-1 or -3 overexpression.

975 **Figure 7 - Figure Supplement 1. Frequency of Netrin ligand and receptor deletions,**
976 **mutations or expression changes in high grade serous ovarian cancer. A)** Oncoprint of
977 genetic alterations in 10 netrin signaling related genes in 398 patients. Alteration types are
978 defined on the right. Only the first 154 patients are shown. **B)** Oncoprint illustrating gene
979 expression outliers among 10 netrin signaling related genes in 201 patients (first 122 patients
980 shown). Genomic data used is from Ovarian Serous Cystadenocarcinoma (TCGA, PanCancer
981 Atlas) (201 samples with RNA seqV2, z-score cut off of 1.5). **C)** TCGA RNA-seq data for
982 HGSOC patients (TCGA PanCancer Atlas study) was used to identify high Netrin-1 or -3 and
983 low Netrin-1 or -3 expressing patients (high expressing are above z-score 1.2). Progression free
984 survival was used to construct Kaplan-Meier plots and survival was compared using a logrank
985 test.

986

987 **Figure 8. Netrin overexpression causes increased dissemination of tumor nodules. A)**
988 Netrin overexpressing and control OVCAR8 cells were injected into the intraperitoneal space of
989 female NOD/SCID mice. Mice were euthanized following 35 days and analyzed for disease
990 burden by necropsy and histopathology. **B)** The spread of cancer to the diaphragm, liver,
991 omentum, and mesometrium was determined from necropsies and colors used in the anatomical
992 schematic correspond with petal plots for each genotype of cells. Petal plot radius illustrates
993 frequency of mice bearing disease spread to a particular location. The radius of color fill is
994 proportional to the total number of animals with tumor nodules found in that location. **C)**
995 Photographs of necropsy findings in the mesometrium. Locations of ovaries (*), oviduct (yellow
996 arrow), and uterine horn (green arrow) are indicated in each case. Tumor nodules are indicated
997 by white arrows. **D)** The number of mesometrium associated tumor nodules was determined for
998 each mouse. Mean values are indicated and differences between genotype were determined by
999 one way anova (* $P<0.05$, ** $P<0.01$). **E)** Photographs of necropsy findings in the liver.
1000 Location of sternum is indicated (#) in each image. Tumor nodules are indicated by white
1001 arrows. **F)** The number of liver associated tumor nodules was determined for each mouse. Mean
1002 values are indicated and differences between genotype were determined by one way anova (**
1003 $P<0.01$, *** $P<0.001$). **G** and **H)** Histology of mesometrial tumor nodules are shown. Serial

1004 sections were stained with H&E, or with the indicated antibodies for immunohistochemistry.
1005 Ovaries are indicated (*), as are the oviduct (yellow arrow), the uterus (green arrow), and the
1006 tumor nodule (white arrow). Scale bar = 2mm

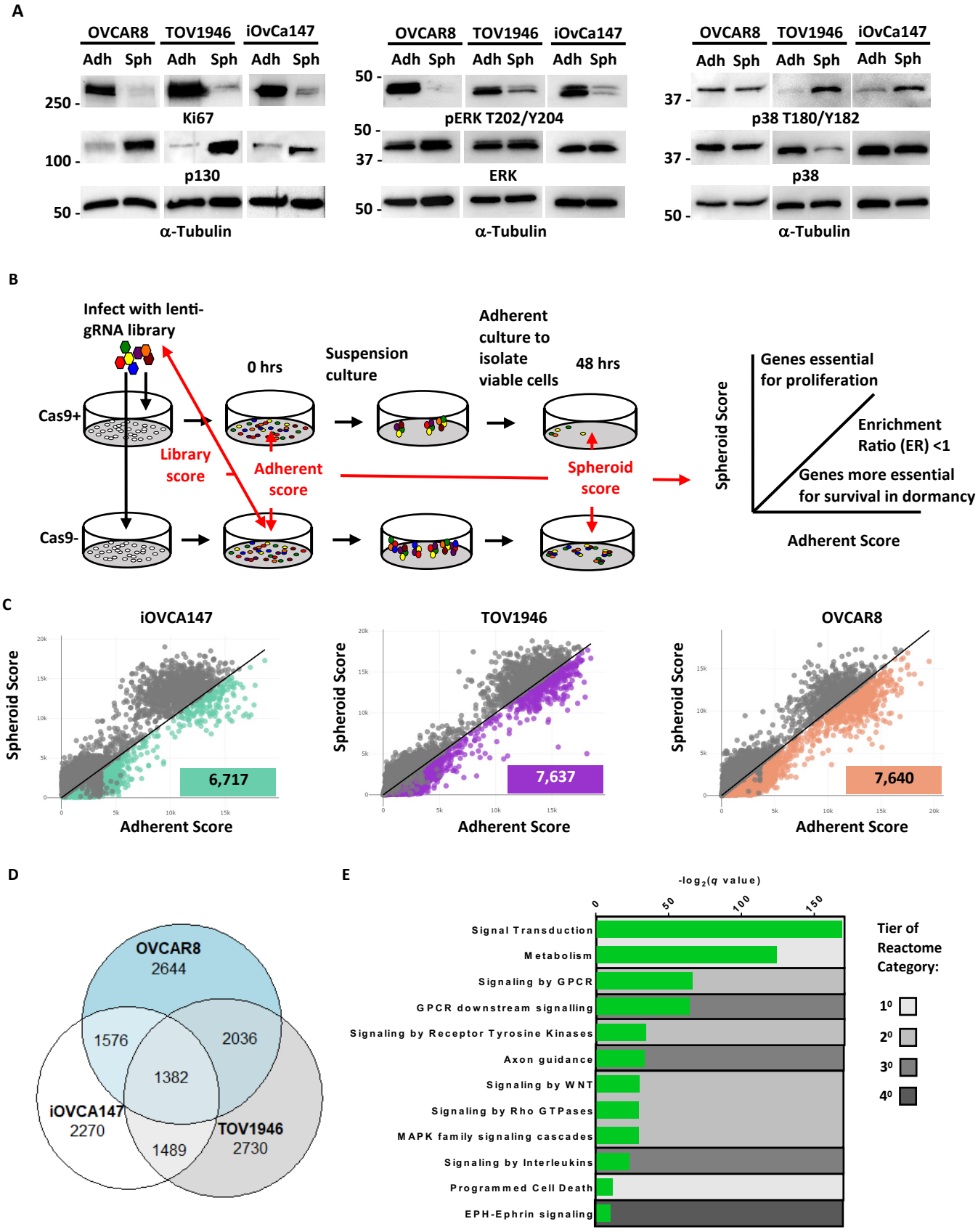
A
OVCAR8
TOV1946
iOvCa147
Adh Sph
250 -
Ki67
100 -
p130
50 -
α-Tubulin
50 -
pERK T202/Y204
37 -
ERK
p38 T180/Y182
p38
B
Infect with lenti-gRNA library
Cas9+
Cas9-
Library score
0 hrs
Adherent score
Suspension culture
Adherent culture to isolate viable cells
48 hrs
Spheroid score
Spheroid Score
Genes essential for proliferation
Enrichment Ratio (ER) <1
Genes more essential for survival in dormancy
Adherent Score
C
iOVCA147
TOV1946
OVCAR8
6,717
7,637
7,640
Adherent Score
D
OVCAR8
2644
1576
2036
1382
iOVCA147
2270
1489
TOV1946
2730
E
-log2(q value)
0
50
100
150
Signal Transduction
Metabolism
Signaling by GPCR
GPCR downstream signalling
Signaling by Receptor Tyrosine Kinases
Axon guidance
Signaling by WNT
Signaling by Rho GTPases
MAPK family signaling cascades
Signaling by Interleukins
Programmed Cell Death
EPH-Ephrin signaling
Tier of Reactome Category:
1⁰
2⁰
3⁰
4⁰

Figure 1

A

TRACS (Toolset for the Ranked Analysis of GO-CRISPR Screens) algorithm:

All Enrichment Scores (ES) for all genes → **Discard genes with Library ES in bottom quartile** → **Compare Spheroid ES and Adherent ES** → **Select genes with negative log2 Spheroid/Adherent ratio, *P*<0.05**

B

Gene scoring formula

Gene score: $$GS_j = \sum_{i=1}^{s} \left(\log_2 \frac{[normalized\ sgRNA\ abundance]_{Cas9+}}{[avg\ normalized\ sgRNA\ abundance]_{Cas9-}} \right)$$

Enrichment score: $$ES_j = \frac{\frac{1}{n}\sum_{i=1}^{n} GS\ rank}{s}$$

Enrichment ratio: $$ER_j = \log_2 \frac{ES_{j_{final}}}{ES_{j_{initial}}}$$

C

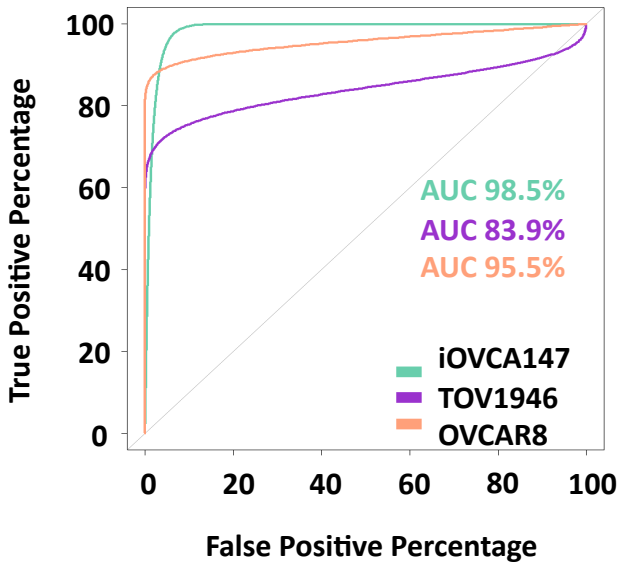

D

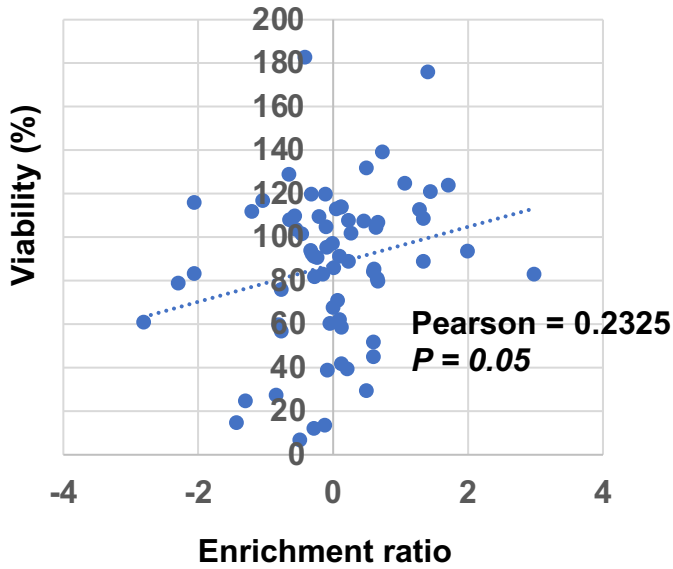

Figure 1 – Figure Supplement 1

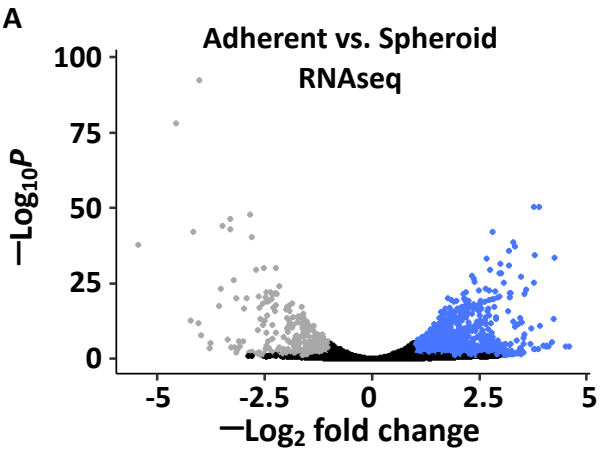

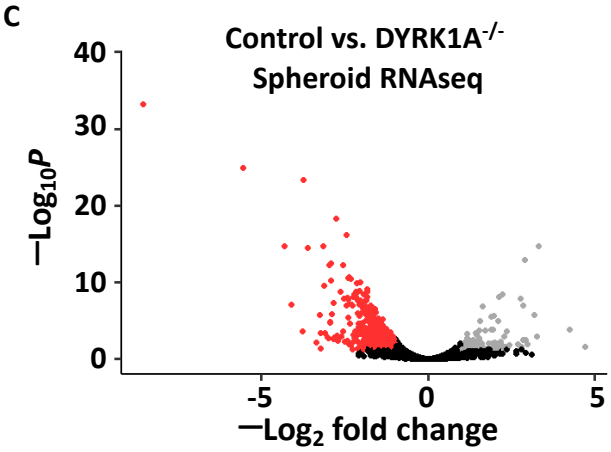

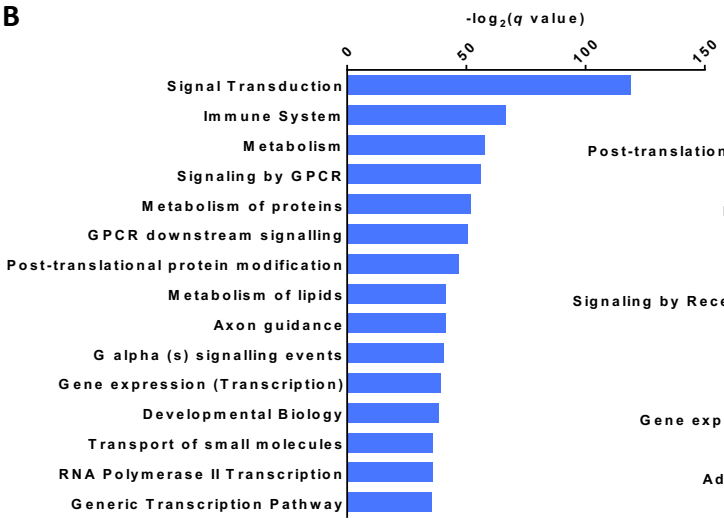

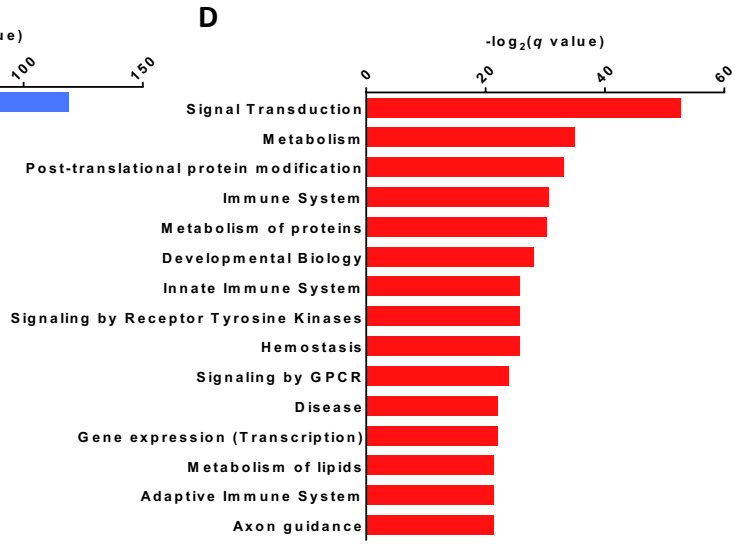

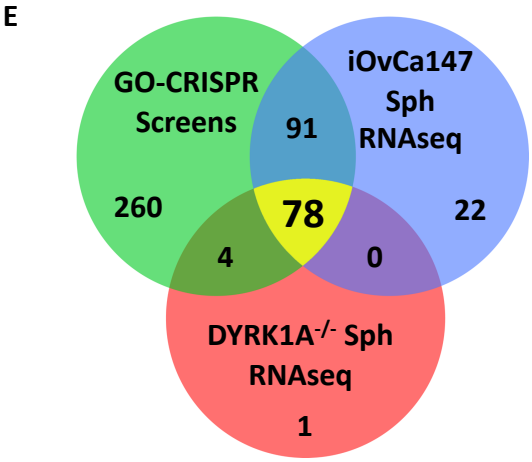

F

Secondary and tertiary Reactome pathways	Rank
Post-translational protein modification	1
Signaling by GPCR	2
GPCR downstream signalling	3
RNA Polymerase II Transcription	4
Innate Immune System	5
Generic Transcription Pathway	6
Adaptive Immune System	7
Axon guidance	8
Cytokine Signaling in Immune system	9
Signaling by Receptor Tyrosine Kinases	10

Figure 2

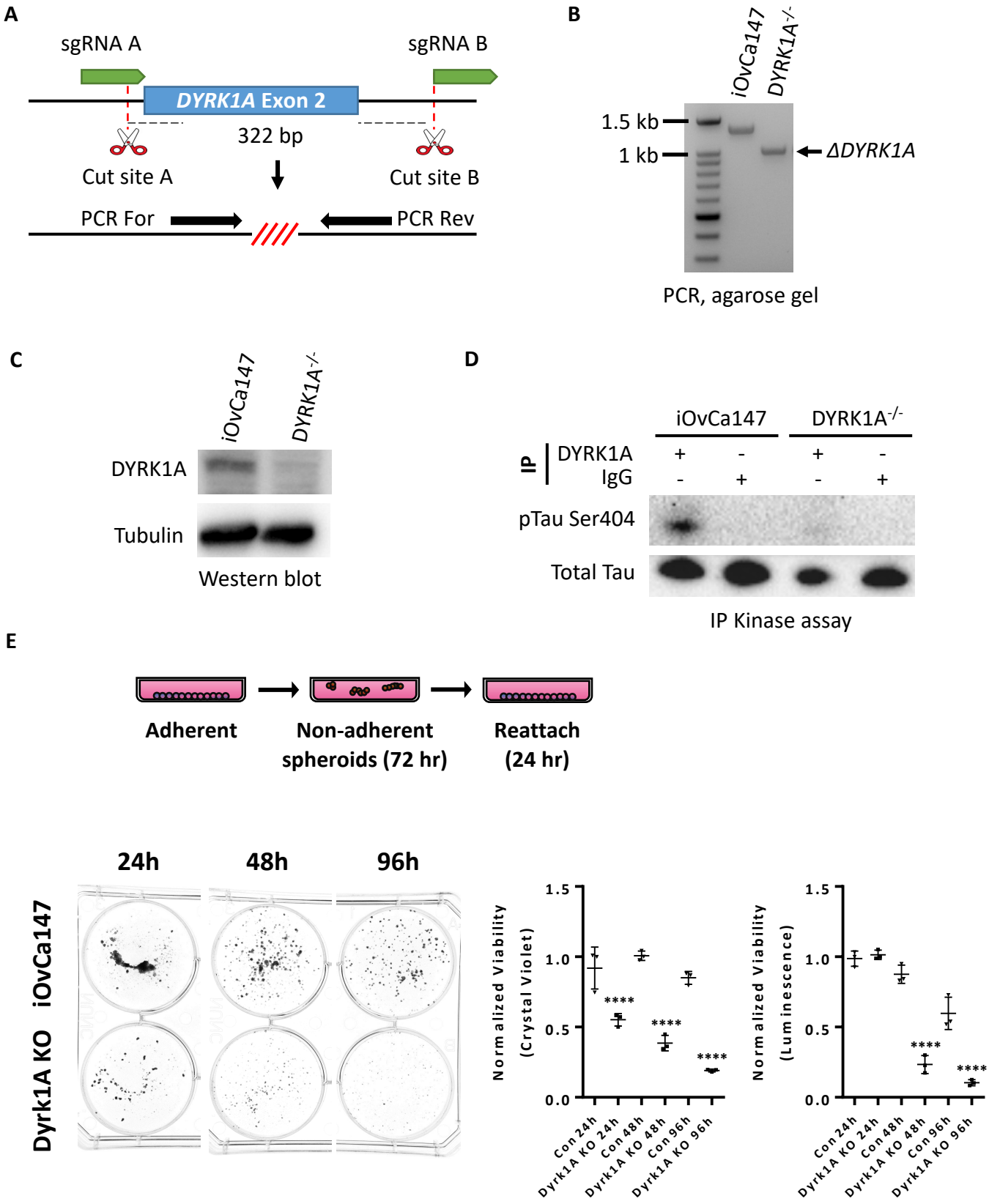

Figure 2 – Figure Supplement 1

A

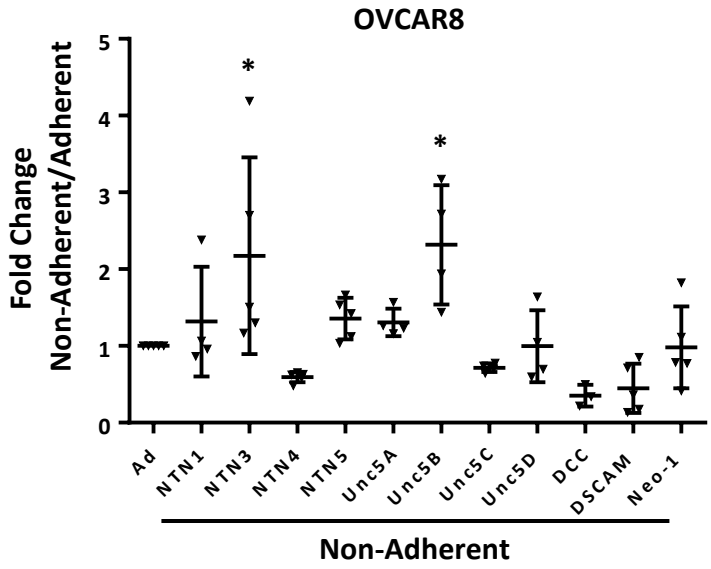
OVCAR8
Fold Change
Non-Adherent/Adherent
0
1
2
3
4
5
*
*
Ad
NTN1
NTN3
NTN4
NTN5
Unc5A
Unc5B
Unc5C
Unc5D
DCC
DSCAM
Neo-1
Non-Adherent

B

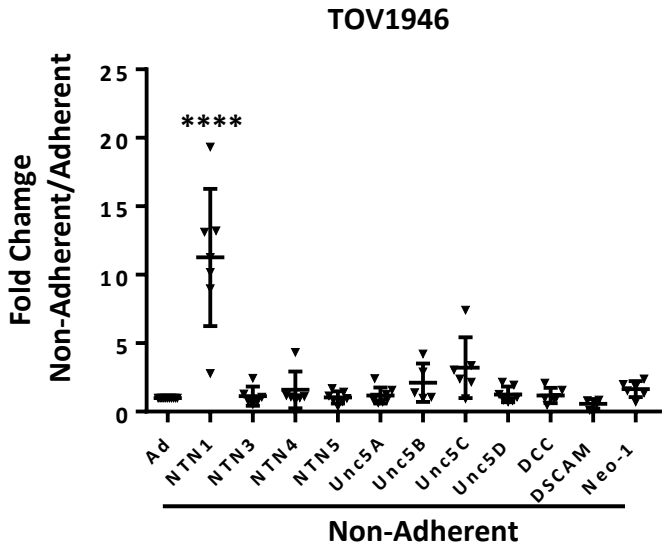
TOV1946
Fold Chamge
Non-Adherent/Adherent
0
5
10
15
20
25
****
Ad
NTN1
NTN3
NTN4
NTN5
Unc5A
Unc5B
Unc5C
Unc5D
DCC
DSCAM
Neo-1
Non-Adherent

C

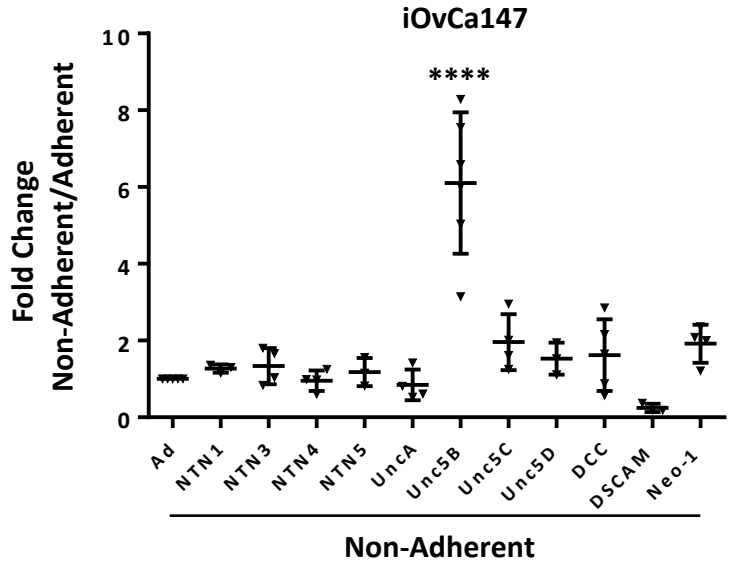
iOvCa147
Fold Change
Non-Adherent/Adherent
0
2
4
6
8
10
****
Ad
NTN1
NTN3
NTN4
NTN5
UncA
Unc5B
Unc5C
Unc5D
DCC
DSCAM
Neo-1
Non-Adherent

Figure 3

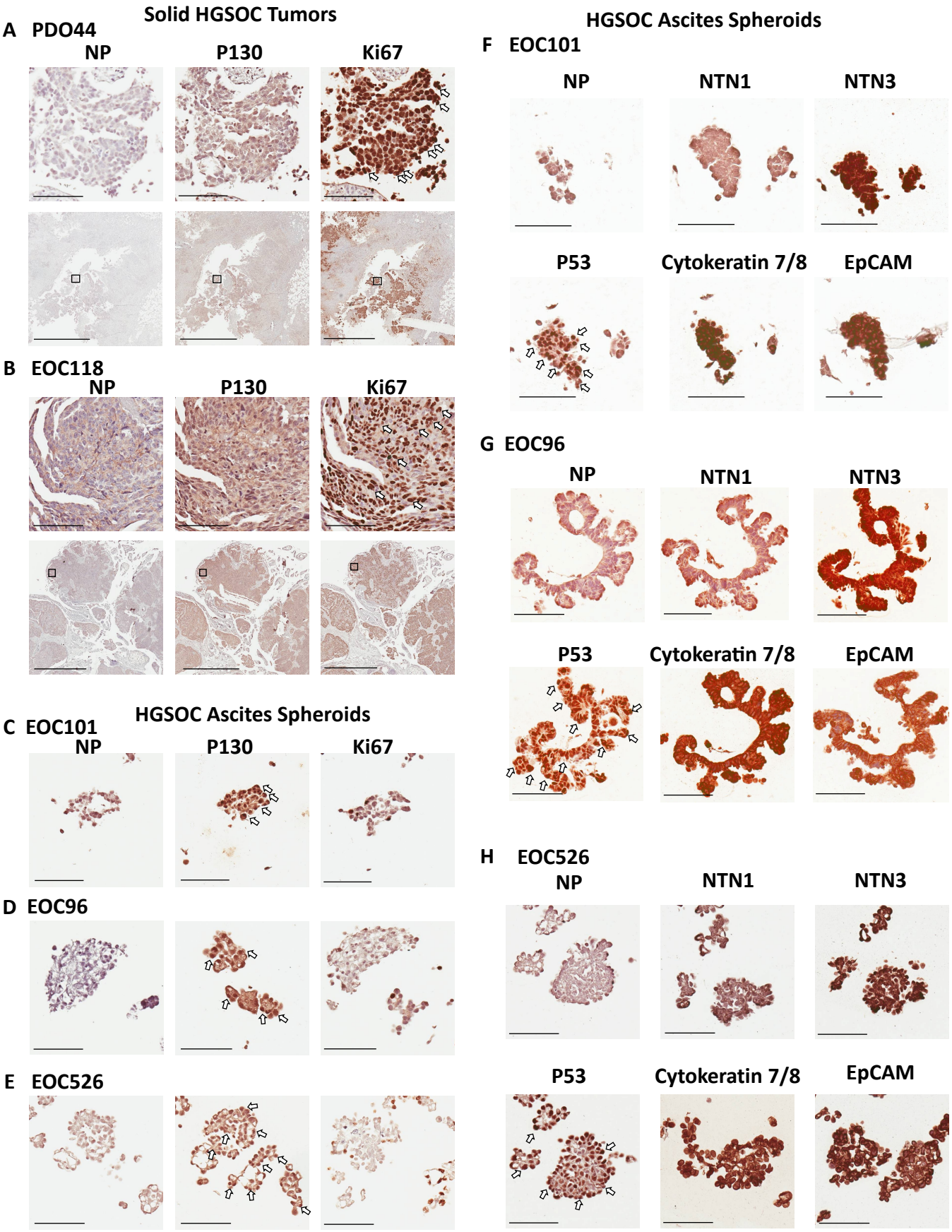
Solid HGSOC Tumors
A PDO44
NP
P130
Ki67
B EOC118
NP
P130
Ki67
HGSOC Ascites Spheroids
C EOC101
NP
P130
Ki67
D EOC96
E EOC526
HGSOC Ascites Spheroids
F EOC101
NP
NTN1
NTN3
P53
Cytokeratin 7/8
EpCAM
G EOC96
NP
NTN1
NTN3
P53
Cytokeratin 7/8
EpCAM
H EOC526
NP
NTN1
NTN3
P53
Cytokeratin 7/8
EpCAM

Figure 4

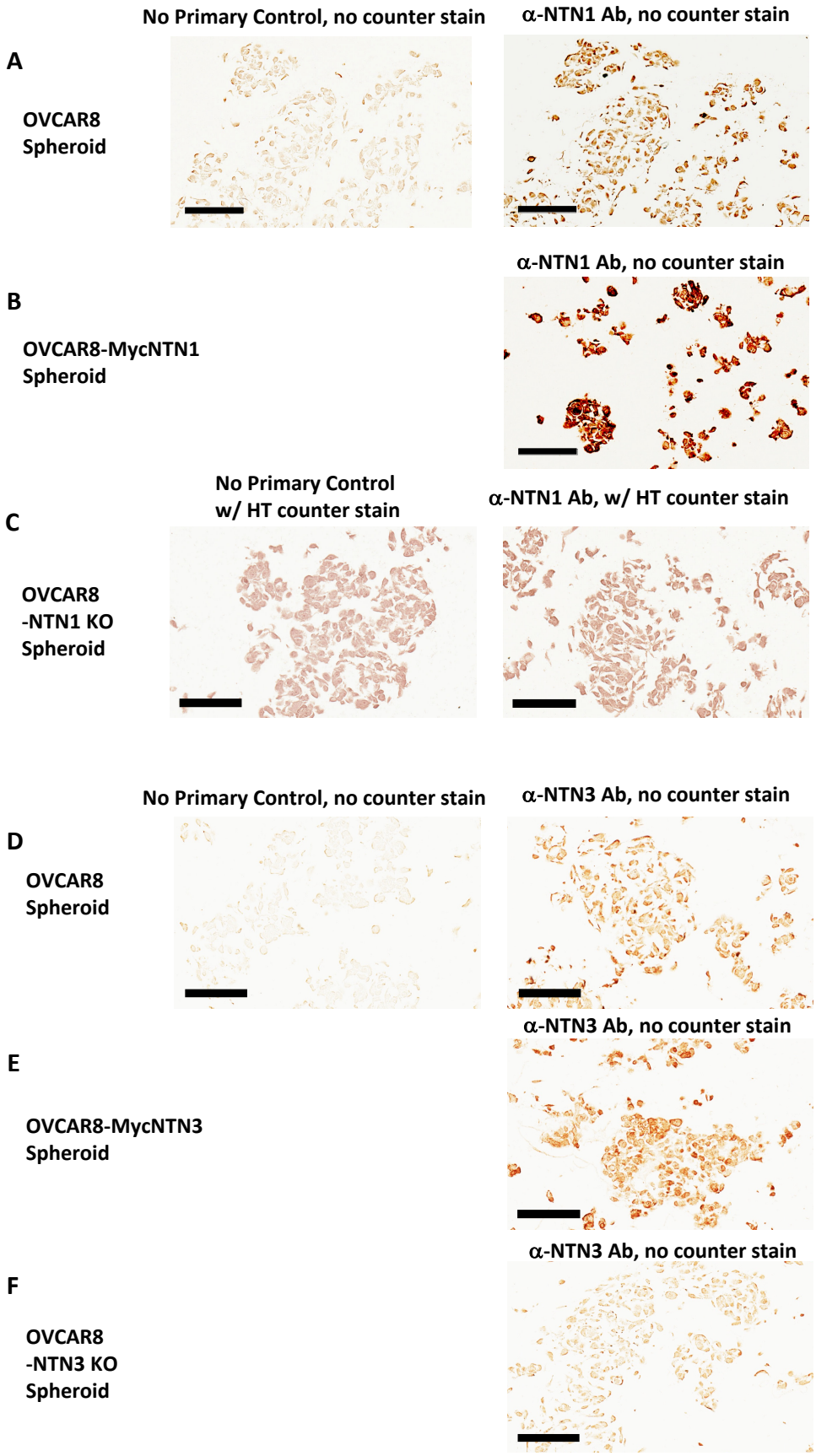

Figure 4 – Figure Supplement 1

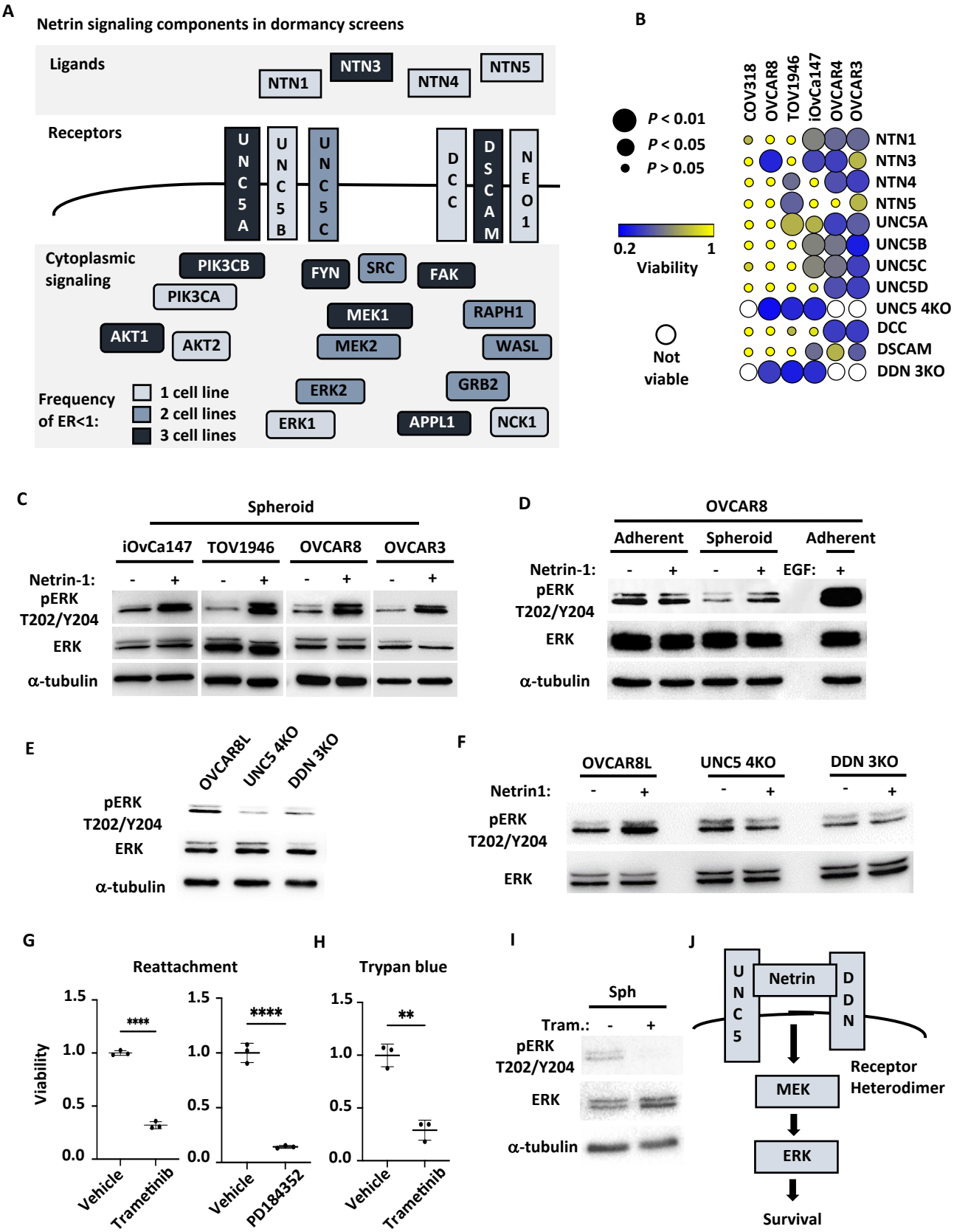
A
Netrin signaling components in dormancy screens
Ligands
NTN1
NTN3
NTN4
NTN5
Receptors
UNC5A
UNC5B
UNC5C
DCC
DSCAM
NEO1
Cytoplasmic signaling
PIK3CB
PIK3CA
FYN
SRC
FAK
MEK1
RAPH1
AKT1
AKT2
MEK2
WASL
ERK2
GRB2
ERK1
APPL1
NCK1
Frequency of ER<1:
1 cell line
2 cell lines
3 cell lines
B
COV318
OVCAR8
TOV1946
iOvCa147
OVCAR4
OVCAR3
P < 0.01
P < 0.05
P > 0.05
0.2
1
Viability
Not viable
NTN1
NTN3
NTN4
NTN5
UNC5A
UNC5B
UNC5C
UNC5D
UNC5 4KO
DCC
DSCAM
DDN 3KO
C
Spheroid
iOvCa147
TOV1946
OVCAR8
OVCAR3
Netrin-1:
pERK T202/Y204
ERK
α-tubulin
D
OVCAR8
Adherent
Spheroid
Adherent
Netrin-1:
EGF:
pERK T202/Y204
ERK
α-tubulin
E
OVCAR8L
UNC5 4KO
DDN 3KO
pERK T202/Y204
ERK
α-tubulin
F
OVCAR8L
UNC5 4KO
DDN 3KO
Netrin1:
pERK T202/Y204
ERK
G
Reattachment
Viability
1.5
1.0
0.5
0.0
****
Vehicle
Trametinib
****
Vehicle
PD184352
H
Trypan blue
**
Vehicle
Trametinib
I
Sph
Tram.:
pERK T202/Y204
ERK
α-tubulin
J
UNC5
Netrin
DDN
Receptor Heterodimer
MEK
ERK
Survival

Figure 5

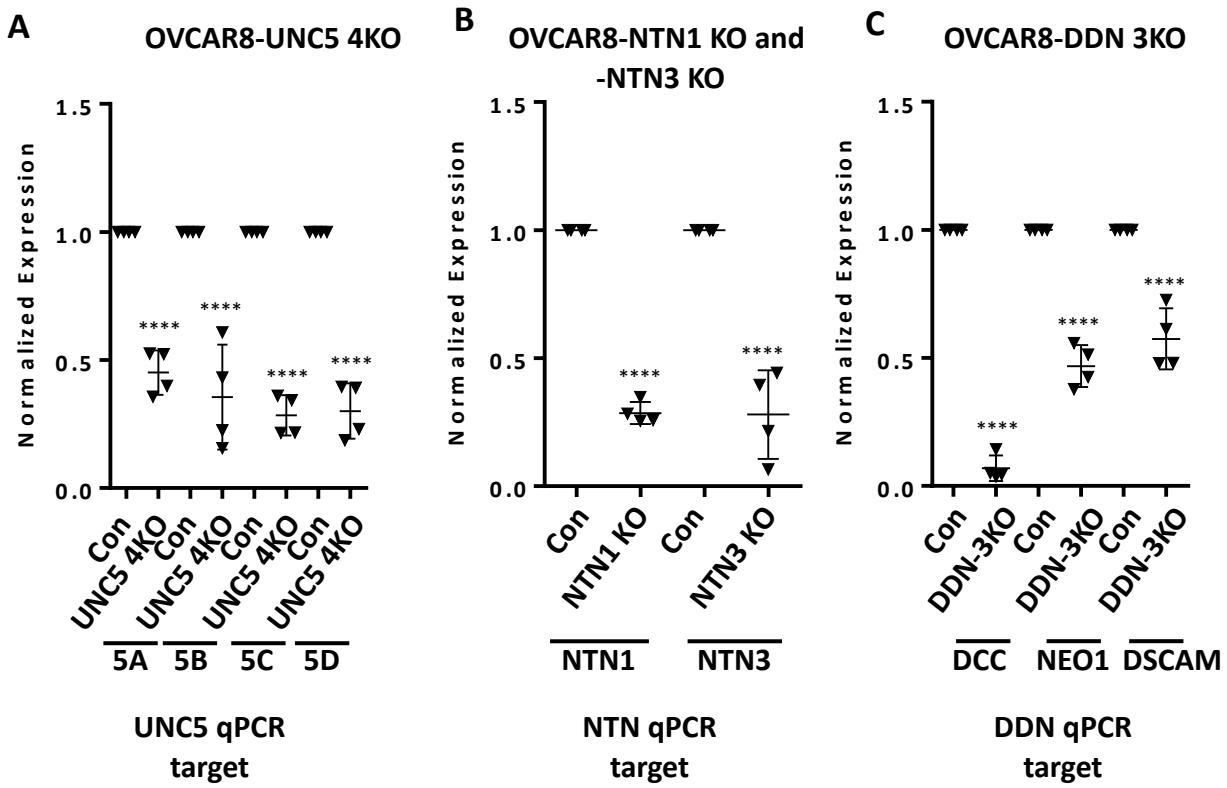

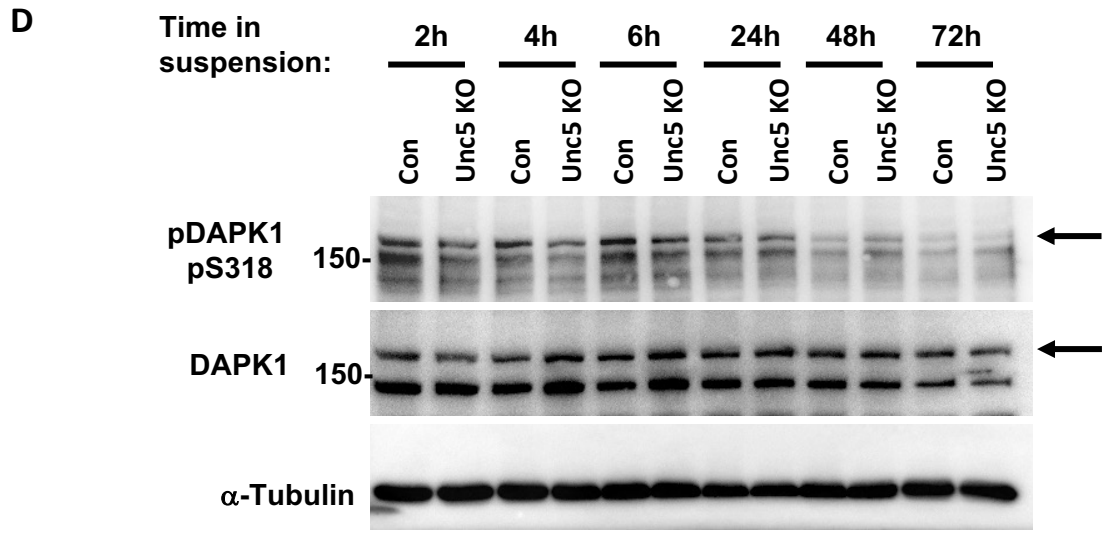

Figure 5 – Figure Supplement 1

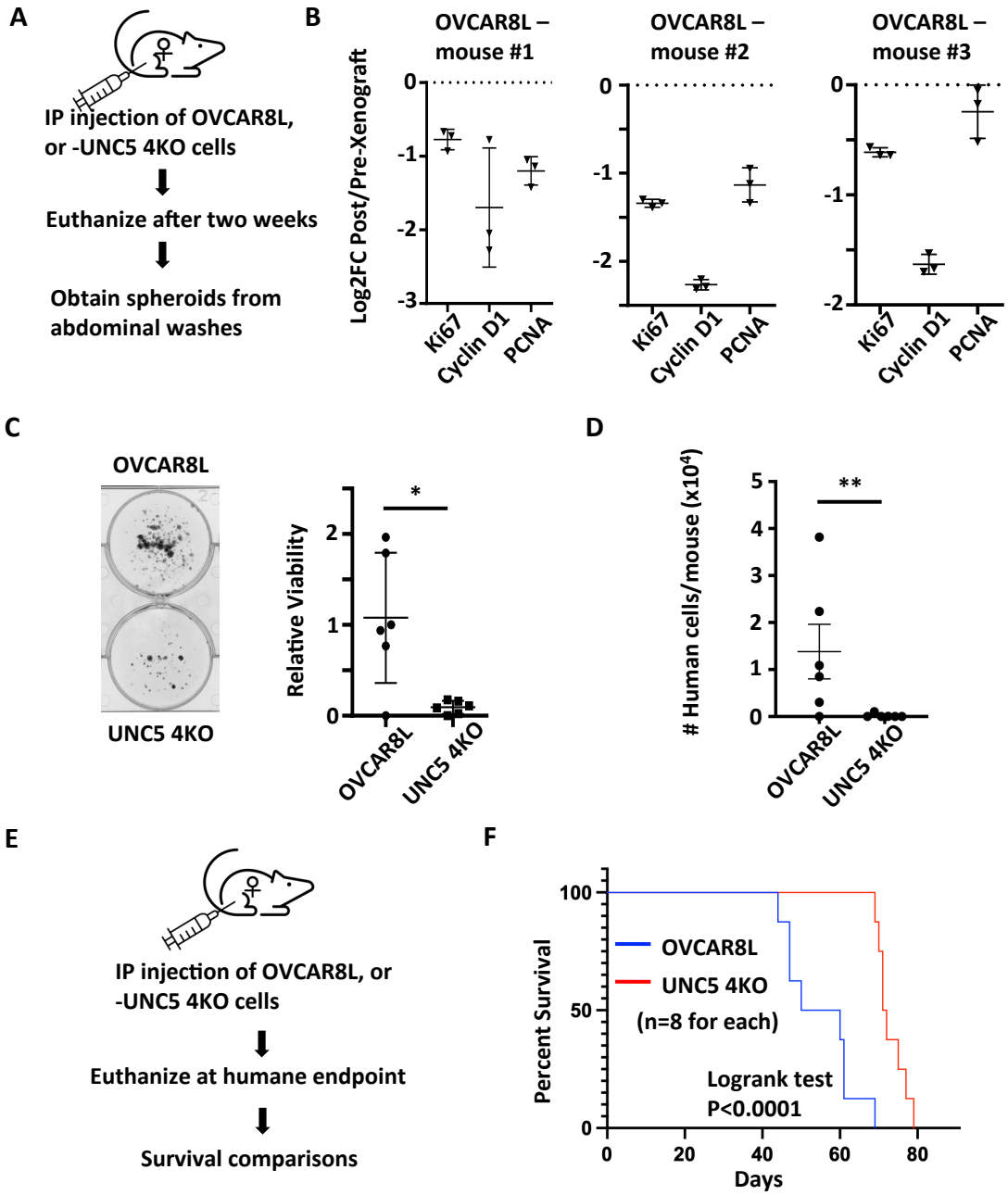
A
IP injection of OVCAR8L, or -UNC5 4KO cells
Euthanize after two weeks
Obtain spheroids from abdominal washes
B
OVCAR8L – mouse #1
OVCAR8L – mouse #2
OVCAR8L – mouse #3
Log2FC Post/Pre-Xenograft
Ki67
Cyclin D1
PCNA
C
OVCAR8L
UNC5 4KO
Relative Viability
OVCAR8L
UNC5 4KO
D
Human cells/mouse (x10⁴)
OVCAR8L
UNC5 4KO
E
IP injection of OVCAR8L, or -UNC5 4KO cells
Euthanize at humane endpoint
Survival comparisons
F
Percent Survival
OVCAR8L
UNC5 4KO
(n=8 for each)
Logrank test
P<0.0001
Days

Figure 6

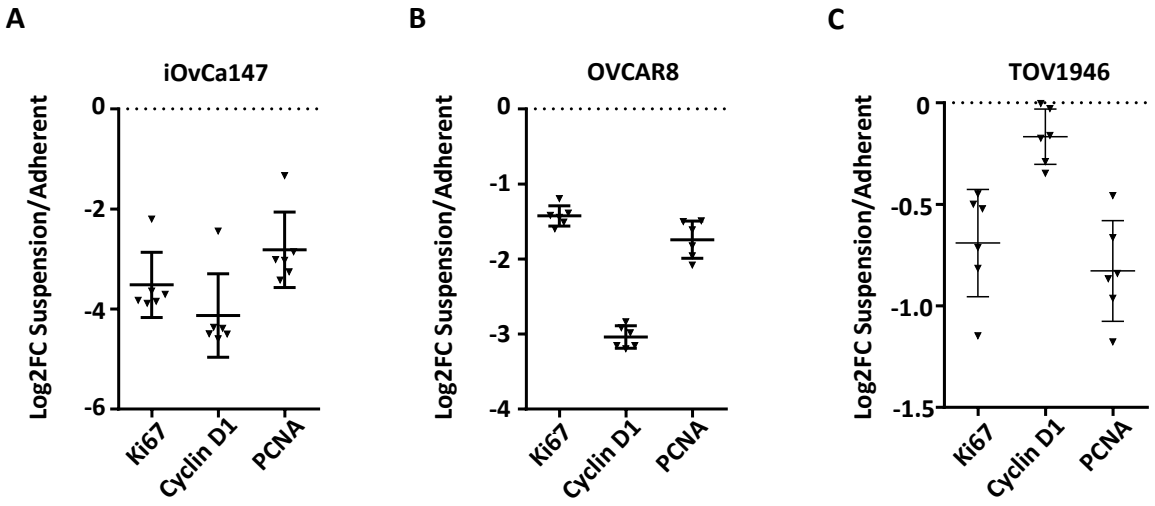

Figure 6 – Figure Supplement 1

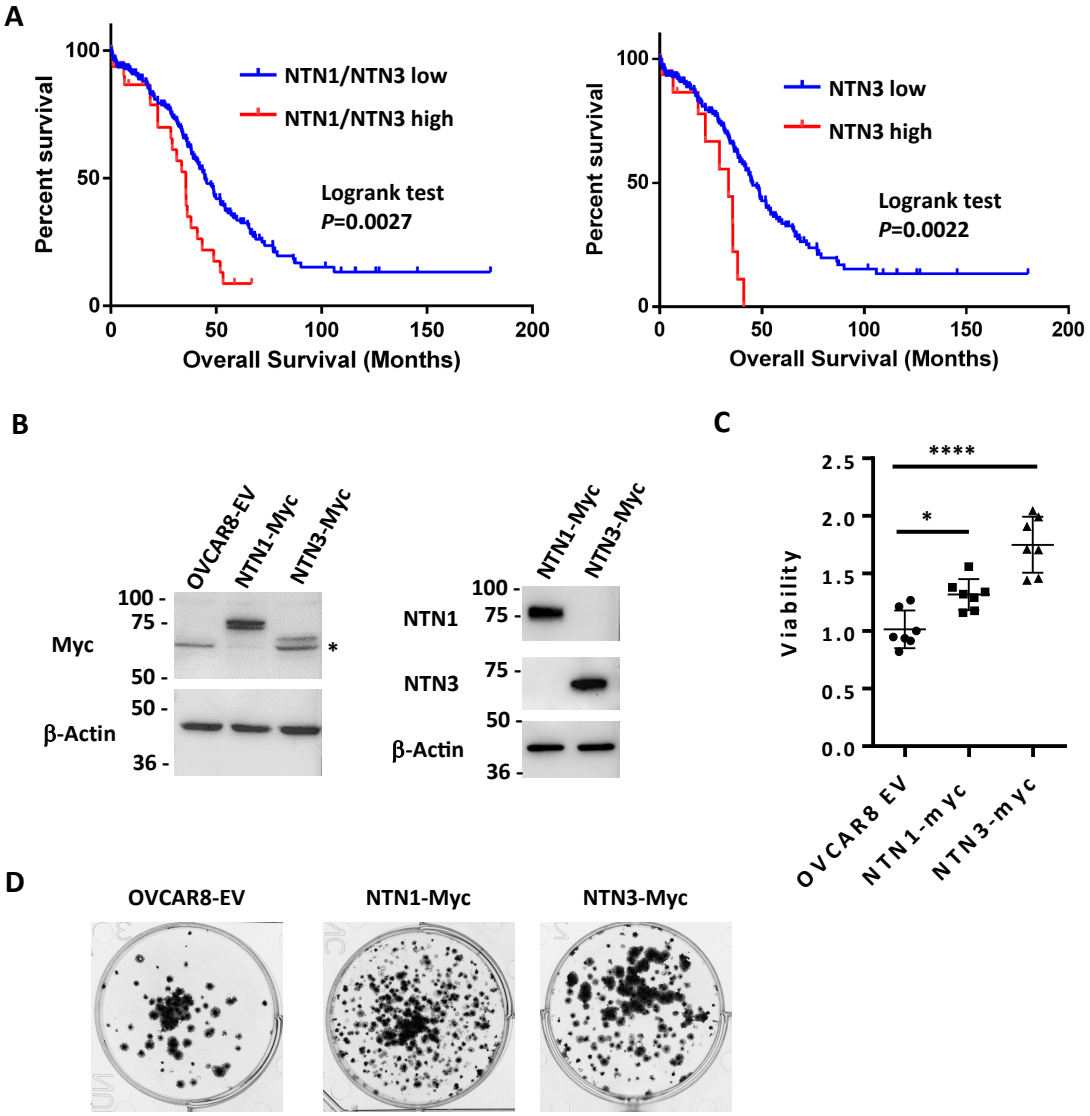
A
Percent survival
NTN1/NTN3 low
NTN1/NTN3 high
Logrank test
P=0.0027
Overall Survival (Months)
NTN3 low
NTN3 high
Logrank test
P=0.0022
B
OVCAR8-EV
NTN1-Myc
NTN3-Myc
Myc
β-Actin
NTN1
NTN3
C
Viability
****
*
OVCAR8 EV
NTN1-myc
NTN3-myc
D
OVCAR8-EV
NTN1-Myc
NTN3-Myc

Figure 7

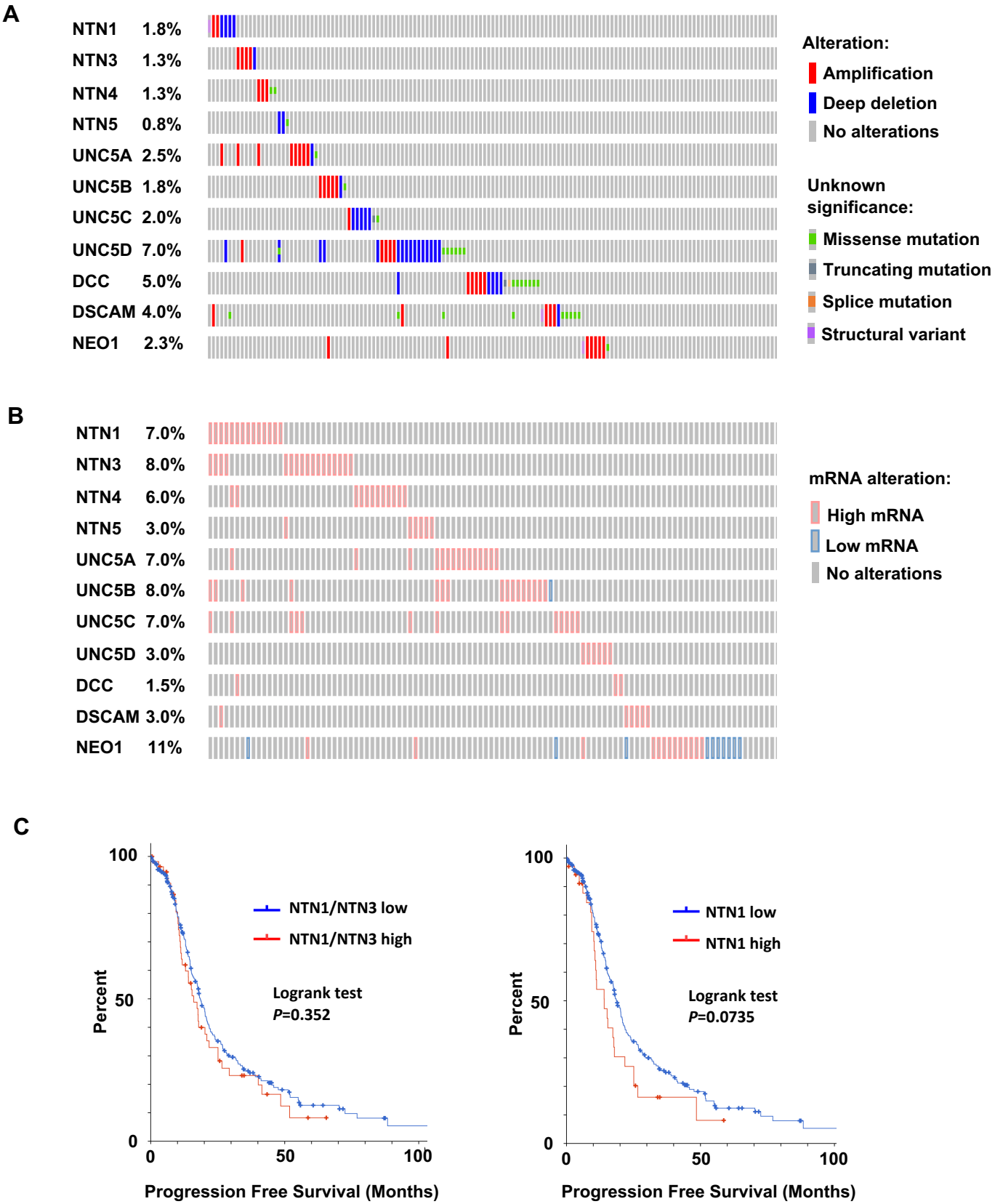

Figure 7 – Figure Supplement 1

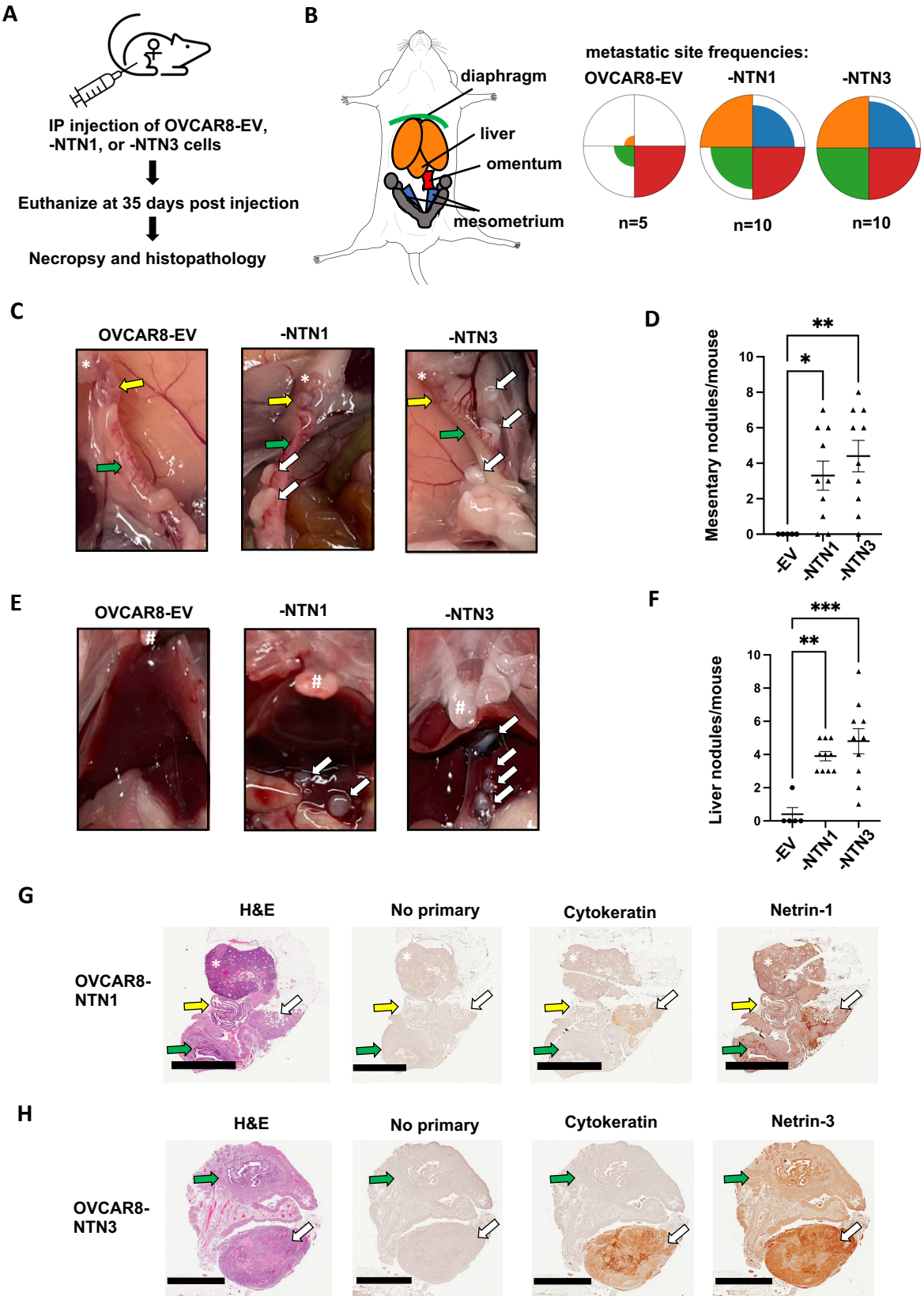
A
IP injection of OVCAR8-EV, -NTN1, or -NTN3 cells
Euthanize at 35 days post injection
Necropsy and histopathology
B
diaphragm
liver
omentum
mesometrium
metastatic site frequencies:
OVCAR8-EV
-NTN1
-NTN3
n=5
n=10
n=10
C
OVCAR8-EV
-NTN1
-NTN3
D
Mesentary nodules/mouse
-EV
-NTN1
-NTN3
E
OVCAR8-EV
-NTN1
-NTN3
F
Liver nodules/mouse
-EV
-NTN1
-NTN3
G
H&E
No primary
Cytokeratin
Netrin-1
OVCAR8-NTN1
H
H&E
No primary
Cytokeratin
Netrin-3
OVCAR8-NTN3

Figure 8